Geoscience Frontiers 11 (2020) 613–634

Contents lists available at ScienceDirect

Geoscience Frontiers

journal homepage: www.elsevier.com/locate/gsf

Research Paper

Integrated model for earthquake risk assessment using neural network and analytic hierarchy process: Aceh province, Indonesia

Ratiranjan Jena [a], Biswajeet Pradhan [a,b,*], Ghassan Beydoun [a], Nizamuddin [c], Ardiansyah [c], Hizir Sofyan [d], Muzailin Affan [c]

[a] Centre for Advanced Modelling and Geospatial Information Systems (CAMGIS), School of Information, Systems and Modelling, University of Technology Sydney, NSW, 2007, Australia
[b] Department of Energy and Mineral Resources Engineering, Choongmu-gwan, Sejong University, 209 Neungdong-ro, Gwangjin-gu, Seoul, 05006, South Korea
[c] Department of Informatics, Syiah Kuala University, Banda Aceh, Indonesia
[d] Department of Statistics, Syiah Kuala University, Banda Aceh, Indonesia

ARTICLE INFO

Handling Editor: Masaki Yoshida

Keywords:
Earthquake
Hazard
Vulnerability
Risk
GIS
ANN–AHP

ABSTRACT

Catastrophic natural hazards, such as earthquake, pose serious threats to properties and human lives in urban areas. Therefore, earthquake risk assessment (ERA) is indispensable in disaster management. ERA is an integration of the extent of probability and vulnerability of assets. This study develops an integrated model by using the artificial neural network–analytic hierarchy process (ANN–AHP) model for constructing the ERA map. The aim of the study is to quantify urban population risk that may be caused by impending earthquakes. The model is applied to the city of Banda Aceh in Indonesia, a seismically active zone of Aceh province frequently affected by devastating earthquakes. ANN is used for probability mapping, whereas AHP is used to assess urban vulnerability after the hazard map is created with the aid of earthquake intensity variation thematic layering. The risk map is subsequently created by combining the probability, hazard, and vulnerability maps. Then, the risk levels of various zones are obtained. The validation process reveals that the proposed model can map the earthquake probability based on historical events with an accuracy of 84%. Furthermore, results show that the central and southeastern regions of the city have moderate to very high risk classifications, whereas the other parts of the city fall under low to very low earthquake risk classifications. The findings of this research are useful for government agencies and decision makers, particularly in estimating risk dimensions in urban areas and for the future studies to project the preparedness strategies for Banda Aceh.

1. Introduction

The destructive power of earthquakes is very strong, has a wide-range effect, and endangers the safety of human lives and properties (Xu and Dai, 2010). Indonesia is one of the highly seismically active countries in the world with severe damage rates (Sørensen and Atakan, 2008). The country has experienced a number of destructive earthquakes in the last two decades. Indonesia consists of several thousands of small islands situated along the continental oceanic plate boundary of the Eurasian plate and Indo–Australian plate in the central part of the Alpine–Himalayan seismic belt (Granger et al., 1999; Petersen et al., 2001). Trends on plate tectonics reveal the Indian plate to be part of the large Indo–Australian plate underlying Bengal Bay and Indian Ocean. The plate motion is towards the northeastern direction with an average speed of 6 cm annually (Sørensen and Atakan, 2008). The plate subducts beneath the Burma plate as a microplate of the large Eurasian plate at the region of Sunda trench (Sørensen and Atakan, 2008). This subduction process creates thrust faults and volcanic activities, the two major reasons of earthquakes in Indonesia (Bellier et al., 1997).

Indonesia has experienced a large number of earthquakes based on historical records and information from the earthquake database of the United States Geological Survey (USGS). The meeting of the tectonic plates produces a reverse fault system governed by regional geology and active volcanos. According to worldwide earthquake databases, 150 or

* Corresponding author. Centre for Advanced Modelling and Geospatial Information Systems (CAMGIS), School of Information, Systems and Modelling, University of Technology Sydney, NSW, 2007, Australia.
E-mail addresses: biswajeet24@gmail.com, Biswajeet.Pradhan@uts.edu.au (B. Pradhan).
Peer-review under responsibility of China University of Geosciences (Beijing).

https://doi.org/10.1016/j.gsf.2019.07.006
Received 3 April 2019; Received in revised form 21 May 2019; Accepted 11 July 2019
Available online 23 July 2019

more earthquakes were experienced from 1900 to 2017. Total fatalities exceeded 266,270 in the last 400 years in different regions of Indonesia. Some high deformation rates have triggered many large earthquake events (≥8.0), such as the 1861 Nias event, 2004 event in the Indian Ocean, and the Simeulue event in 2005 (ISMNPD, 2004). The Sumatra–Andaman megathrust earthquake in 2004 is the second largest magnitude earthquake recorded to date (Bilham and Ambrasey, 2005). The earthquake created a rupture of 1300 km (length) characterized by seven separate segments from the northwest to the Andaman Islands at more than 1600 km (Bilham and Ambrasey, 2005). The earthquake duration is the longest event period recorded at approximately 600 s. Youngs et al. (1997) and Lin and Lee (2008) explained that the intertectonic subduction of the plate was associated with the event and bedrock movement. In Indonesia, the recorded human toll in Aceh province and North Sumatra due to the 2004 earthquake was approximately 110,229 deaths, 12,123 missing, and 703,518 displaced (Siemon et al., 2005). The details of fatalities and injuries are presented in Table 1. Infrastructure damage due to the dominant disastrous earthquakes may be due to the use of poor construction materials. Damage to buildings was caused by the earthquake magnitudes (i.e., ≥ 8.0) that used to frequently occur in Aceh province, thus continuously affecting the city of Banda Aceh (ISMNPD, 2004; Irwansyah, 2010). The total damage estimated for the buildings accounted for 35% of total buildings (ISMNPD, 2004; Siemon et al., 2005).

Banda Aceh is the capital city of Aceh province that is exposed potentially to a significant earthquake vulnerability and risk along the major fault of Great Sumatran Fault (GSF). GSF is a right-lateral strike-slip fault that has not experienced any large earthquake in the northern part of the fault particularly in Banda Aceh from the last 200 years (Irwansyah, 2010). This tranquil part of the fault is considerably recognized as a seismic gap in Aceh province (Irwansyah, 2010). An accumulation of increased stress along the GSF may be observed due to the collision between plates. Petersen et al. (2001) mentioned the capability of GSF for producing up to $M = 7.9$ event, as the history explained the capability of $M = 7.7$ that has occurred along this fault. This earthquake occurred in 1892 near the city of Sibolga (approximately ±570 km at the southeast of Banda Aceh) (Petersen et al., 2001; Siemon et al., 2005). Furthermore, Banda Aceh is situated on thick sedimentary alluvium deposits (Siemon et al., 2005). However, the site amplification probability is extremely high in the thick alluvium (Brebbia et al., 1996; Setiawan, 2017; Setiawan et al., 2018). Therefore, estimate the seismic site amplification of Banda Aceh is required by recognizing the probability of future earthquakes because the city is surrounded by several earthquake events (Lin and Lee, 2008). The city has experienced ground shaking due to some major earthquakes in the recent years. Moreover, understanding Banda Aceh's vulnerability and risk due to earthquakes is essential and significant for urban planning (Zhang and Jia, 2010). The probability, hazard, and social vulnerability analysis can be applied in future risk mapping and decision management by considering the risk reduction, prevention, and mitigation (Davidson and Freudenburg, 1996; Davidson, 1997; Davidson and Shah, 1997; Turner et al., 2003; Wisner et al., 2003; Adger et al., 2004; Yücemen et al., 2004; Rygel et al., 2006; Birkmann, 2007; Pradhan and Jena, 2016; Pradhan et al., 2018; Setiawan et al., 2018). In the current analysis, the hazards and vulnerability resulting in high ability and stand on socially operated attributes and contexts, for a large population, are unsheltered. Research scholars and scientists have divergent definitions for the notion of vulnerability and risk because of the complexity behavior (Cutter, 1996; Adger et al., 2004; Tierney, 2006; Khan, 2012; Hosseini et al., 2014; Beccari, 2016). Very few similar studies have been conducted for earthquake vulnerability assessment using GIS technique and not any detailed analysis has been conducted for risk assessment (Bathrellos et al., 2017; Alizadeh et al., 2018a, b). However, the novelty in this work lies in the proposed integrated scheme, which can provide a comprehensive analysis of probability, hazard, vulnerability and risk with good accuracy that can be used for urban planning; a future strategy to reduce the impact and the work describes the strength, limitations and applicability of the developed model. This paper would be useful for model developers, seismic researchers, scientists, academicians, and research scholars.

The remainder of the article is structured as follows. Section 2 describes the related literature review. Sections 3 and 4 describe the study area and data acquisition. Section 5 explains the details of the developed methodology with the architecture. Section 6 provides the details of results and discussion. Section 7 concludes the paper with major concluding remarks.

2. Previous works on earthquake prediction and probability, vulnerability, and risk assessment

We divide this section into three subsections. The first subsection discusses about earthquake probability mapping and forecasting. The second subsection provides a brief description of vulnerability, and the third section provides the overview of risk assessment using various methods.

Avoiding earthquakes may be impossible, but accurate predictions and early warning can reduce the effect of the damage and consequences. Research shows that natural hazards, such as earthquakes, are measured by probabilities, which explain the identification of potential zones for earthquakes in a semi quantitative analysis (Wang et al., 2006). Hazard is the probability of an earthquake in a specific geographic position within a period, and the intensity of ground shaking crosses a given threshold. Artificial neural network (ANN) has a wide range of applications, ranging from civil engineering (Karunanithi et al., 1994) to image processing (McIlraith and Card, 1997) and to geology and seismology (Zhao and Takano, 1999). ANN has been used in earthquake prediction and probability by calculating the importance of seismicity indicators for small and large events (Panakkat and Adeli, 2007). Researchers have used different ANN architectures for earthquake prediction. A recurrent neural network was developed by Panakkat and Adeli (2009) for the prediction of earthquake time and location by using eight seismicity indicators (e.g., T (time), α (latitude), and μ (days)). Moreover, they analyzed several sets of events and computed the latitude and longitude of the location of epicenter, as well as the occurrence time for the same events. Pradhan and Lee (2009, 2010) used ANN model for the landslide hazard and risk assessment using remote sensing and GIS. Turmov et al. (2000) developed earthquake-induced tsunami prediction models using the measurement of electromagnetic and elastic waves simultaneously. Shimizu et al. (2008) studied earthquake forecasting using the technique of sample-entropy based on the VAN method.

The concept of vulnerability is associated with exposure to disaster, which is a prerequisite for risk mapping (Tierney, 2006). More recently, Zebardast (2013) proposed the hybrid factor analysis approach and analytic network process model for projecting a composite social vulnerability index by aggregating the vulnerability indicators. The main objective in this research was to develop a hybrid firefly algorithm (FA) and analytical network process (ANP), (F'ANP) model for the assessment of social vulnerability and to apply in county scale. Gulkan and Sozen (1999) developed a model for seismic vulnerability of concrete and masonry buildings. They explained their methods through the ratios of column and walls using graphical representation. Pay (2001) proposed a novel method for the seismic vulnerability assessment of buildings using the discriminant technique analysis in Turkey. The success rate achieved by Pay was approximately 71.1%. Yakut et al. (2003) proposed another model for the earthquake vulnerability assessment of the reinforced concrete buildings. The method was similar to that of Pay. However, statistical analysis was included in their model. They achieved an accuracy of 80.3% for the highly damaged buildings. Bahadori et al. (2017) developed an integrated model best suited for the assessment of seismic vulnerability of buildings in Mahabad City in Iran. The methodology is an integration of five parameters, such as geotechnical, social, seismological, distance to dangerous facilities, and access to vital facilities along with the sub-parameters. Zhang et al. (2017) described the construction

Table 1
Fatalities and injuries in different regions of Indonesia due to earthquake events.

No.	Year	Region	Fatalities	Injuries	Remarks	Sources
1	2018	Sulawesi, Java, Sulawesi Lombok, Sumatra	2828	12,566	Landslides, tsunami, aftershock, foreshock, building damage, widespread fatalities	NGDC, NOAA, USGS
2	2017	Java, Ambon	5	36		
3	2016	Sumatra	104	1273	Heavy damage in Aceh region	NOAA
4	2015	Papua	1		Buildings damaged or destroyed	NOAA
5	2013	Sumatra	43	276		USGS
6	2012	Wharton Basin	12	12	Doublet & building damage	
7	2011	Sumatra	10			
8	2010	Sumatra, Papua	425	62	Tsunami (local), hundreds missing	
9	2009	Sumatra, Java, Talaud, West Papua	1201	4266	Severe damage, Local tsunami, doublet	NGDC
10	2008	Sulawesi, Simeulue	7	59		USGS
11	2007	Sumatra, Molucca Sea	95	548		USGS
12	2006	Sumatra, Java, Seram	6428	47,867	Tsunami (Local & regional), extreme damage	
13	2005	Sumatra	1314	1146		USGS
14	2004	Sumatra–Andaman, Papua, Alor, Western New Guinea, Bali	228,002	629	Tsunami (basin wide), severe damage, doublet, several thousand buildings damaged	NGDC
15	2003	Halmahera	1		Extensive damage	
16	2002	Sumatra, Western New Guinea	11	65	Tsunami & damage	
17	2000	Sumatra, Sulawesi	149	2438	Tsunami & destruction	NGDC
18	1996	Biak, Sulawesi	174	423	Local tsunami	
19	1995	Sumatra	84	1868	Extreme damage	NGDC
20	1994	Java, Sumatra	457	2000+	Tsunami	NGDC
21	1992	Flores	2500	500	Severe damage (Tsunami)	
22	1989	West Papua	120	125		
23	1984	Sumatra		1		
24	1982	Flores	15	390		
25	1981	Papua	305		Thousands missing	
26	1979	Bali	30	200+		
27	1977	Sumba	180	1100	Tsunami(local)	
28	1976	Bali, Papua	995	4750	Landslides, thousands missing	USGS, NGDC
29	1968	Sulawesi	213			
30	1965	Sanana	73			
31	1943	Sumatra, Java	213	2096	Extensive damage	NGDC
32	1938	Banda Sea			Local tsunami	
33	1935	Sumatra			Local tsunami	
34	1917	Bali	1500		Landslides	
35	1899	Seram	3864		Destructive	
36	1867	Java	8		Extensive damage	NGDC
37	1861	Sumatra	2000+			
38	1852	Banda Sea			Severe damage	NGDC
39	1833	Sumatra	1000+		Tsunami (local)	
40	1815	Bali	10,253		Tsunami	NGDC
41	1797	Sumatra	1000+		Tsunami(local)	USGS
42	1699	Batavia (Jakarta)	30		Building collapsed	
43	1674	Ambon Serem	89	135	Tsunami & building damage	NGDC
44	1629	Banda Sea			Regional tsunami	

of an evaluation model for the most significant assessment of social vulnerability using a rough set up based on catastrophe progression. Karimzadeh et al. (2017) prepared a Vs30 map by applying an indirect approach using geological and topographical data in Iran. Alizadeh et al. (2018a, b) developed a new model for the earthquake urban vulnerability and tested it for the Tabriz City of Iran. They observed reasonably good results due to the use of hybrid ANN and analytic hierarchy process (AHP) approach. They achieved an accuracy of 90%. Alizadeh et al. (2018a, b) and Panahi et al. (2014) proposed a model for the seismic vulnerability assessment of the urban buildings in Tabriz City of Iran by using the Multi Criteria Decision Making (MCDM) approach.

Zhihuan and Junjing (1990) applied fuzzy logic in their research on damage and risk assessment. Mili et al. (2018) proposed a holistic model for earthquake risk assessment (ERA) and determining the risk reduction and management priorities in urban areas. Chaulagain et al. (2015) presented the estimation of structural vulnerability and successfully analyzed the risk and the expected economic losses for future earthquakes in Nepal. They used the Open Quake-engine for earthquake hazard and risk in Nepal. Ram and Guoxin (2013) explained the seismic ground motion that has been estimated by a probabilistic approach in Nepal. They also calculated the peak ground accelerations (PGAs) using seismic source information and probabilistic parameters in their study. Khan et al. (2018) estimated the earthquake risk for developing countries using the modern ERA methods in their article. They analyzed Pakistan as a case study. They successfully estimated the earthquake risk using a practical event-based PSHA method.

The motivation of this study indicates that Aceh is a seismic-prone province on Sumatra with devastating seismic events that resulted in severe casualties and damages (Petersen et al., 2001). Banda Aceh is considered a high-risk zone for future seismic events because of its unique geographical location, geostructural features, and quaternary sedimentary rocks (Siemon et al., 2005; Irwansyah, 2010). Historical analysis shows that the city has experienced severe ground shaking due to devastating events (ISMNPD, 2004; Irwansyah, 2010). On the basis of the probabilistic and deterministic approach, seismologists and geologists believe that strong events may hit the city in near future because of the release of the accumulated stress in the seismic gap (Irwansyah, 2010). Thus, proposing further studies to generate risk assessment models at the city-scale is necessary. Unfortunately, much fewer studies are conducted at the city level by which an accurate assessment of probability, hazard, and risk can be conducted (e.g., Kafle, 2006; Gitamandalaksana, 2009; Johar et al., 2013). Second, no comprehensive model has been developed for Banda Aceh for a detailed ERA. However, a literature review suggests that risk assessment and urban population risk estimation is necessary to minimize the consequences and severity (Wisner et al., 2003; Ram and Wang, 2013; Zebardast, 2013; Chaulagain

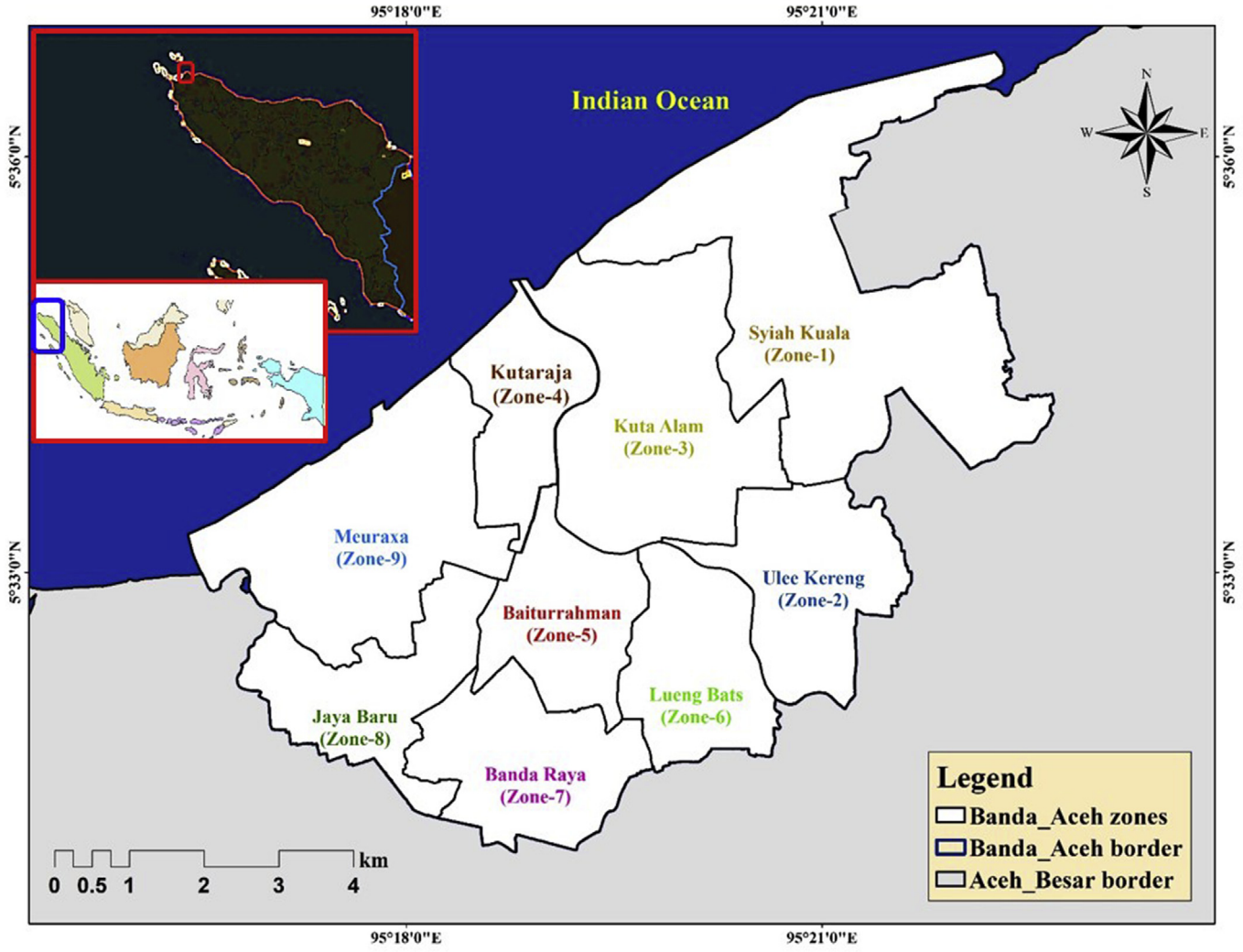

Fig. 1. Location map of study area.

et al., 2015). To achieve this goal, this study (1) develops an integrated model that combines ANN and AHP methods to produce an earthquake risk map; (2) applies and assesses the dimensions of earthquake probability, hazard, and vulnerability for Banda Aceh; and (3) estimates the urban population risk quantitatively and qualitatively. This research is expected to help to reduce the earthquake impact by mapping the risk zones and categorizing them into multiple classes.

3. Study area

The study area is located at 5°33′0″N and 95°19′0″E. The capital of Aceh province is Banda Aceh, and it is the largest city. The city is located at an elevation of approximately 35 m m.s.l. The city covers an area of approximately 61.4 km^2 based on the 2010 census; the city is populated with 219,070 and 250,227 people based on the 2015 census (Johar et al., 2013; Yuzal et al., 2015). Moreover, 10 ethnic groups can be found in the city, of whom the Acehnese is the largest group that comprises approximately 80%–90% of the total population (Yuzal et al., 2015). The most noticeable Aceh fault is the measured structural discontinuity that passes through Banda Aceh. The Aceh fault is active; however, no events are experienced historically inside Banda Aceh. Banda Aceh was affected by a 7.7 magnitude earthquake near the city in the NE region. The study area is presented in Fig. 1.

The geology of Banda Aceh is composed of limestone, phyllite, and slate (Culshaw et al., 1979). These rocks in the Cretaceous age in the geological timescale, and the morphology indicates the mountainous structure at the end of the northern Barisan range in Sumatra (Culshaw et al., 1979). Massive and moderately weathered limestones are specifically found in this range. In the western part of the Indrapuri, mixed lithic conglomerates can be found at the outcrops. The wedges of conglomeratic outcrops are placed between the limestone and the Quaternary deposits and are believed to be of the Palaeogene age (Culshaw et al., 1979). Fossiliferous sandstone deposits can be found in the upper valley of Pliocene or early Pleistocene. These deposits show a shallow water marine environment, thereby serving as evidence of a rise in elevation up to 90 m m.s.l. due to the tectonic upliftment (Johar et al., 2013). In the western side of the Krueng Aceh valley, the unconformable Quaternary sedimentary deposits can be found. Banda Aceh is characterized by quaternary sedimentary deposit along with some patches of peridotitic rocks. Therefore, the Krueng Aceh valley forms a graben-type structure between the Semangko fault and the splay main fault system (Culshaw et al., 1979; Wang et al., 2006).

4. Data

For ERA, data are generally used from single or multiple sources. Freely available earthquake data can be collected from several public and private agencies. These sources are accessible from the Internet and include the Advanced National Seismic System, United States Geological Survey (USGS), National Earthquake Information Center (NEIC), and the

Table 2
Selected layers from literature and data types used in this study.

Criteria	Selected layers	Scale	Type	Resolution (m)
Susceptibility	Slope Curvature Elevation Aspect Epicenter density Epicenter distance Depth density Magnitude distribution PGA density Lithology Amplification factor Fault density Distance from fault	1:30000	Raster layers	5
Hazard	Earthquake Intensity			
Vulnerability	Building density District office Educated people Environmental infrastructure Stadium University Chiefs Service centers Offices Population Transport nodes			

Northern California Earthquake Data Center. We have collected the complete earthquake catalog from USGS and NEIC of various magnitudes with coordinates of latitude between 2°30′00″N and 5°00′00″N and longitude between 94°30′00″E and 99°00′00″E. The probability and vulnerability assessment are extremely challenging without considering the significant criteria and the important indicators that depend on the heterogeneity of the study location. The most vital and useful part of the approach is to select the criteria and indicators adequately to obtain an accurate risk map for Banda Aceh. The details of the criteria and indicators used for this research are presented in Table 2. Data for the probability, hazard, and vulnerability assessment were collected from various national and international agencies such as Statistics Indonesia (www.bps.go.id/eng), GeoNetwork (http://www.fao.org/geonetwork), and the USGS (https://earthquake.usgs.gov). On the basis of the objective and purpose of the study, collected data were used to prepare several layers that were identified and selected after the extensive literature review. A map can transform the qualitative raw data such as opinions of people, observations and documents but it's not easy to be crunched by a statistical software. This can be performed by uncovering emerging patterns, concepts, themes and insight logics. It needs a linked analytic framework and classification techniques to clarify the underlying process and construct a map. However, quantitative data can be represented through choropleth maps or proportional maps using statistical software (http://www.pbcgis.com/normalize/).

5. Methodology

5.1. The integrated ANN–AHP model

The developed model is constructed according to ANN with AHP to conduct ERA. This section describes the different components of the proposed model. We focus specifically on the architecture of the model. The model consists of two main phases that combined ANN and AHP methodology. However, the subsections of ANN are (1) ANN design, (2) MLP algorithm, and (3) training and testing; those for AHP are (1) AHP design, (2) various steps, and (3) implementation are described below. The overall methodological flowchart is given in Fig. 2.

5.2. ANN architecture

Conceptually, the best definition of an ANN is a model that provides output is a combination of some linear or non-linear inputs (Nedic et al.,

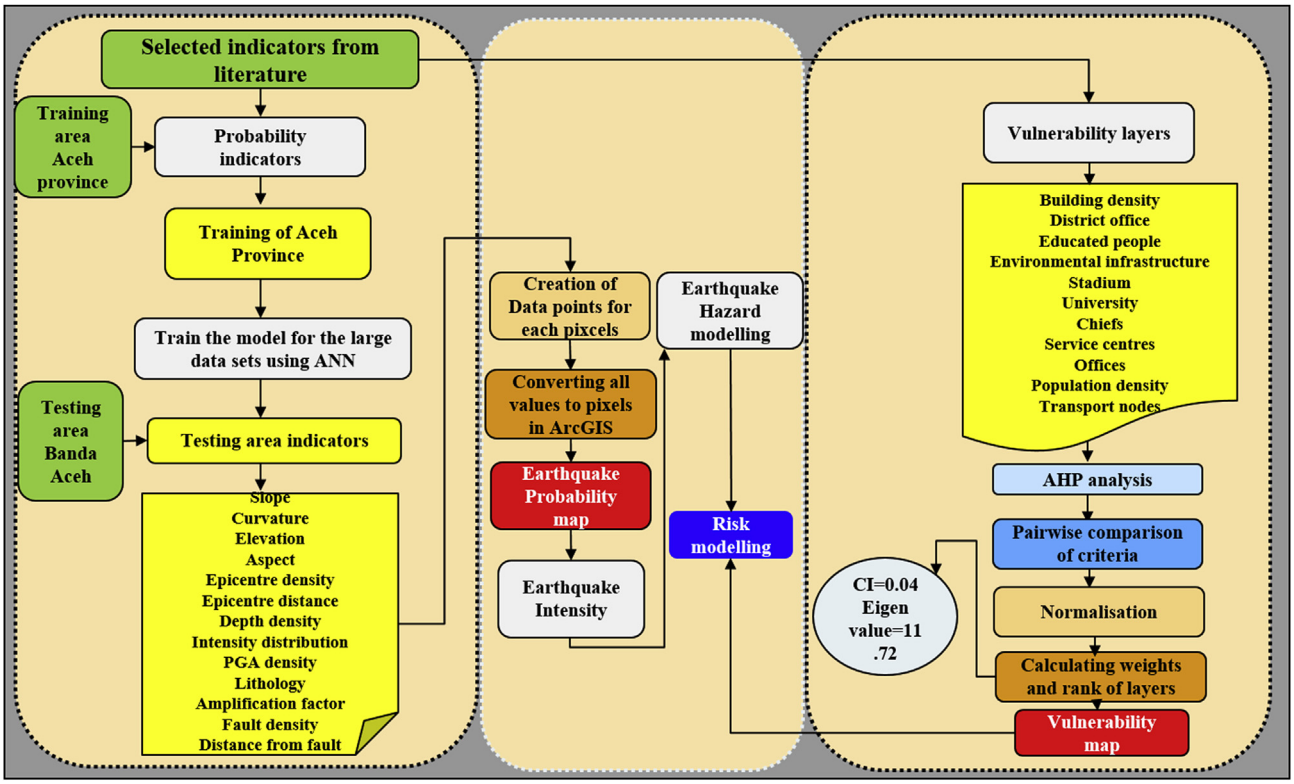

Fig. 2. Methodological flowchart of the developed model.

2014). The mathematical algorithm of ANN is explained by several researchers (Hagan et al., 1996; Saaty, 2013). The most popular and widely used ANN is the multilayer perceptron (MLP) ANN model. An MLP is characterized by three layers, namely, input, hidden, and output layers (Nedic et al., 2014). Fig. 3 shows the framework of the ANN that was applied in this study. Different data that were collected from several sources, such as thematic data, were fed as the input layer in ANN modeling. The trial and error approach will recognize the number of hidden layers and the number of neurons in the network (Saaty, 2013; Nedic et al., 2014). Determination of output layer neurons depends on the application and class analysis type. Each neuron inside the hidden layers begins interacting with the weight of the input neurons and processes the data by linking to each other.

The processed network travels in a single "forward" direction (Pradhan and Lee, 2009). Errors propagate in a backward direction towards the inner ones to adjust the layer values.

Different steps of back-propagated ANN are described below (Zhao and Takano, 1999; Pradhan and Lee, 2010):

1. Initialization: Set all the weights and biases to small real random values.
2. Presentation of input and desired outputs: Present the input vector $x(1)$, $x(2)$,…, $x(N)$ and corresponding desired response $d(1)$, $d(2)$,…, $d(N)$, one pair at a time, where N is the number of training patterns.
3. Calculation of actual outputs through the multilayer perceptron system.

The details of the multilayer perceptron are described below.

$$x_j^{(0)} = \rho\left(S_j^{(l)}\right) \text{ and } S_j^{(l)} = \sum_{i=0}^{ni-1} \omega_{ji}^{(1)} x_i^{(l-1)} \tag{1}$$

The output probability is denoted as $\{\widehat{y_j}\}$ and is assumed as $\{\widehat{y_j}\} = \{x_j^{(L)}\}$ for all $j = 1, 2, \ldots, n_L$. The mean square error (MSRE) for the network can be expressed as $\frac{e^2}{nL}$ where $e_j = y_j - \widehat{y_j}$ is the error signal for the j**th** output. Moreover, the instantaneous squared error can be calculated by $e^2 = \sum_{j=1}^{n\,L} e_j^2$. Therefore, in the learning part, the BP approach minimizes the squared error by varying $\{\omega_{ji}^{(l)}\}$ as per the gradient search method, repetitively. The jth segment connected with the derivatives of squared error in the layer l is expressed by

$$\delta_j^{(1)} = -\frac{1}{2}\frac{\delta e^2}{\delta S_i^{(1)}} \tag{2}$$

Then, these derivatives can be formulated as

$$\delta_j^{(1)} = \begin{cases} \rho'\left(S_j^{(l)}\right)\cdot e_j & \text{for } l=L \\ \rho'\left(S_j^{(l)}\right)\cdot \sum_{i=1}^{n\,l+1} \omega_i^{(l+1)}\cdot\delta_i^{(l+1)} & \text{for } l=L-1,\ L-2,\ldots,1 \end{cases} \tag{3}$$

Eventually, the weights of the MLP are reorganized at the kth instant as

$$\omega_{ji}^{(l)}(k+1) = \omega_{ji}^{(l)}(k) + \Delta_{ji}^{(l)}(k) \quad \text{and} \quad \Delta_{ji}^{(l)}(k) = \mu\delta_i^{(l)} x_i^{(l-1)} + \gamma\delta_{ji}^{(l)}(k-1) \tag{4}$$

where μ is learning rate and γ signify momentum rate hyper-parameters.

5.3. Neural network training and testing

Two sets of data are generally used for the analysis, namely, "training set" and "test set", which are needed for the ANN modeling. The former is applied to develop possible network weights properly by considering the input and output links by the learning algorithm. The performance of the trained network can be verified by applying the "test set" of data. Suitable data preparation is important in the accuracy for the training site of the resultant probability map. The selection of acceptable parameters is important during the training phase (Nedic et al., 2014; Alizadeh et al., 2018a). For the training, we collected complete earthquake data from the USGS site with various magnitude. For ANN, the model needs a huge amount of training data. However, the collected data may not be sufficient for modeling. Thus, the designed model in this research proposes a developed training strategy. The collected data used for training and trained are based on ANN.

5.4. AHP architecture

Thomas L. Saaty developed analytical hierarchy process (AHP) in the 1970s, and it has been applied as a hierarchically structured technique for organizing and analyzing the complex decisions (Panahi et al., 2014). AHP has a wide range of applications in decision-making processes such

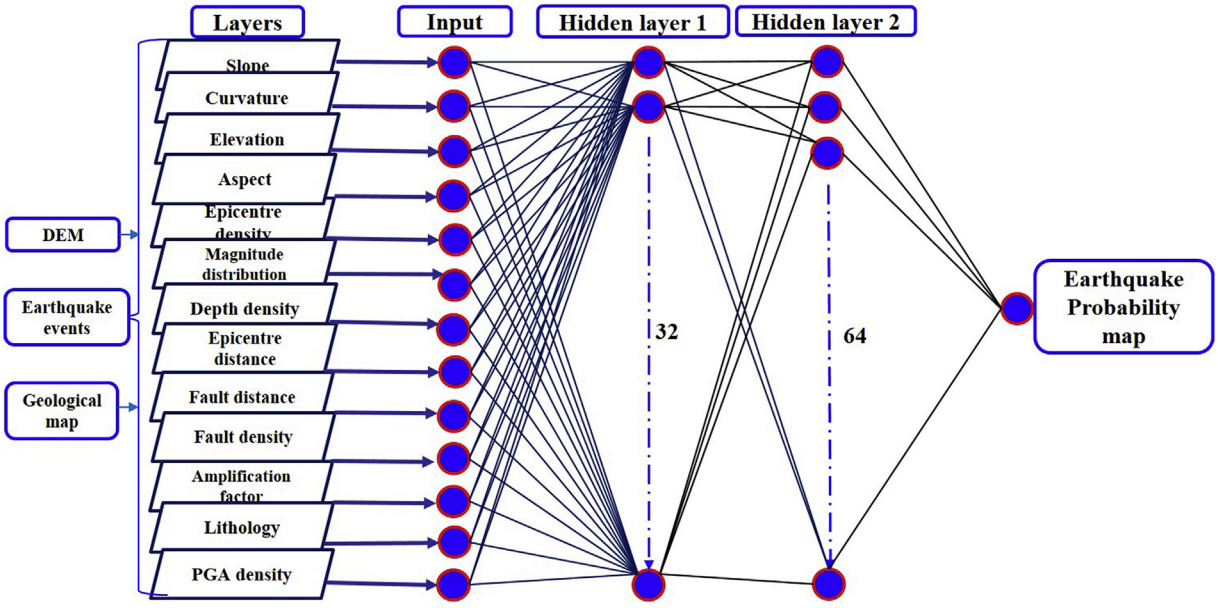

Fig. 3. ANN architecture for earthquake probability analysis.

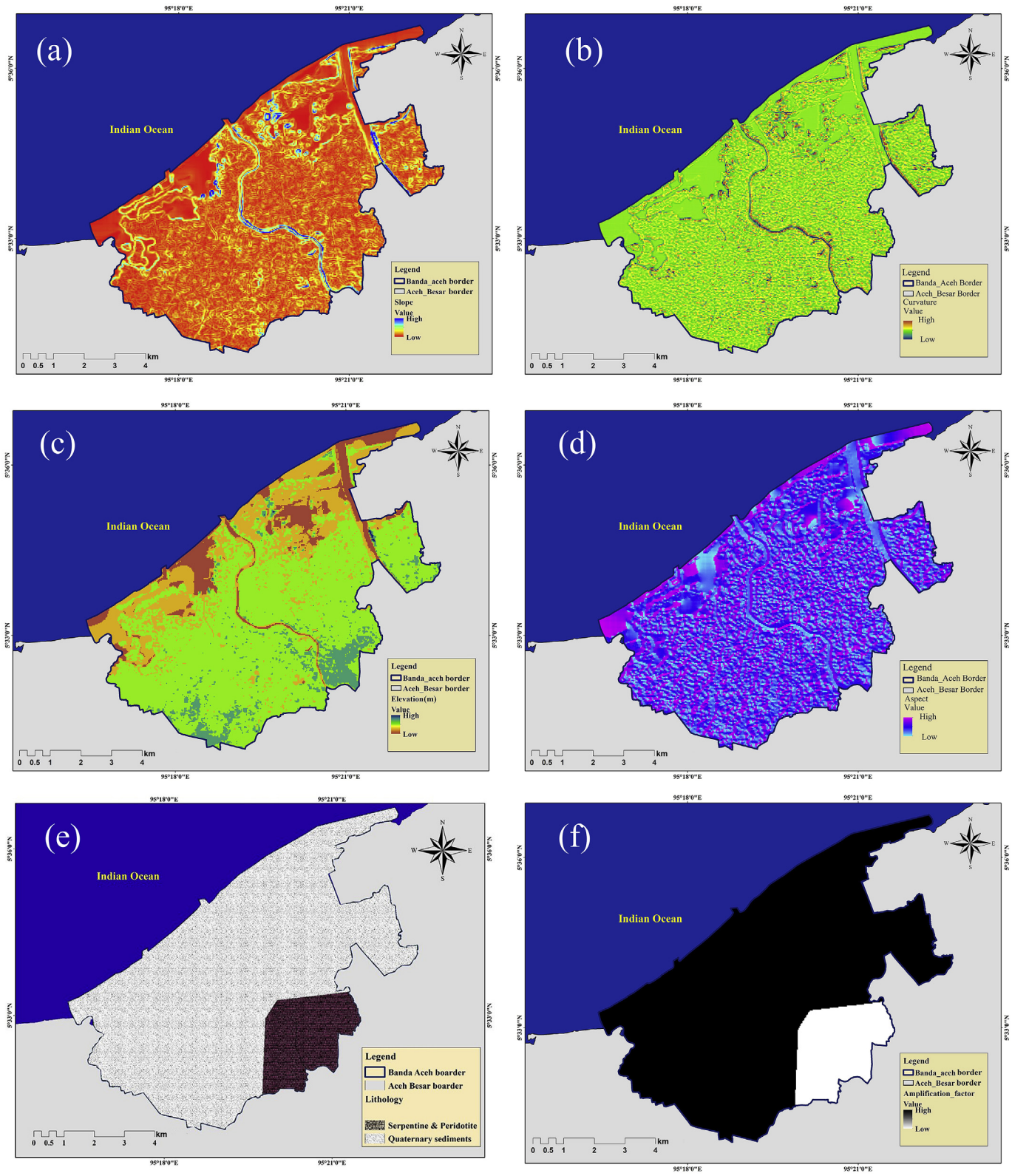

Fig. 4. Criteria for probability mapping using ANN. (a) Slope, (b) curvature, (c) elevation, (d) aspect, (e) lithology, (f) amplification factor, (g) distance from faults, (h) fault density, (i) depth density, (j) epicenter density, (k) PGA density, (l) magnitude density, and (m) distance from epicenter.

as vendor selection, project prioritization, selection of technology, site selection, and decision making (Panahi et al., 2014, Alizadeh et al., 2018a). The AHP approach assists decision makers to observe and notice the one that is suitable for their problems and goals. The numerical values resulted from the subjective evaluations are applied to rank each alternative data layer using a numerical scale. The details of the methodology can be described in the following steps (Paola and Schowengerdt, 1995; Gong, 1996; Atkinson and Tatnall, 1997; Abraham,

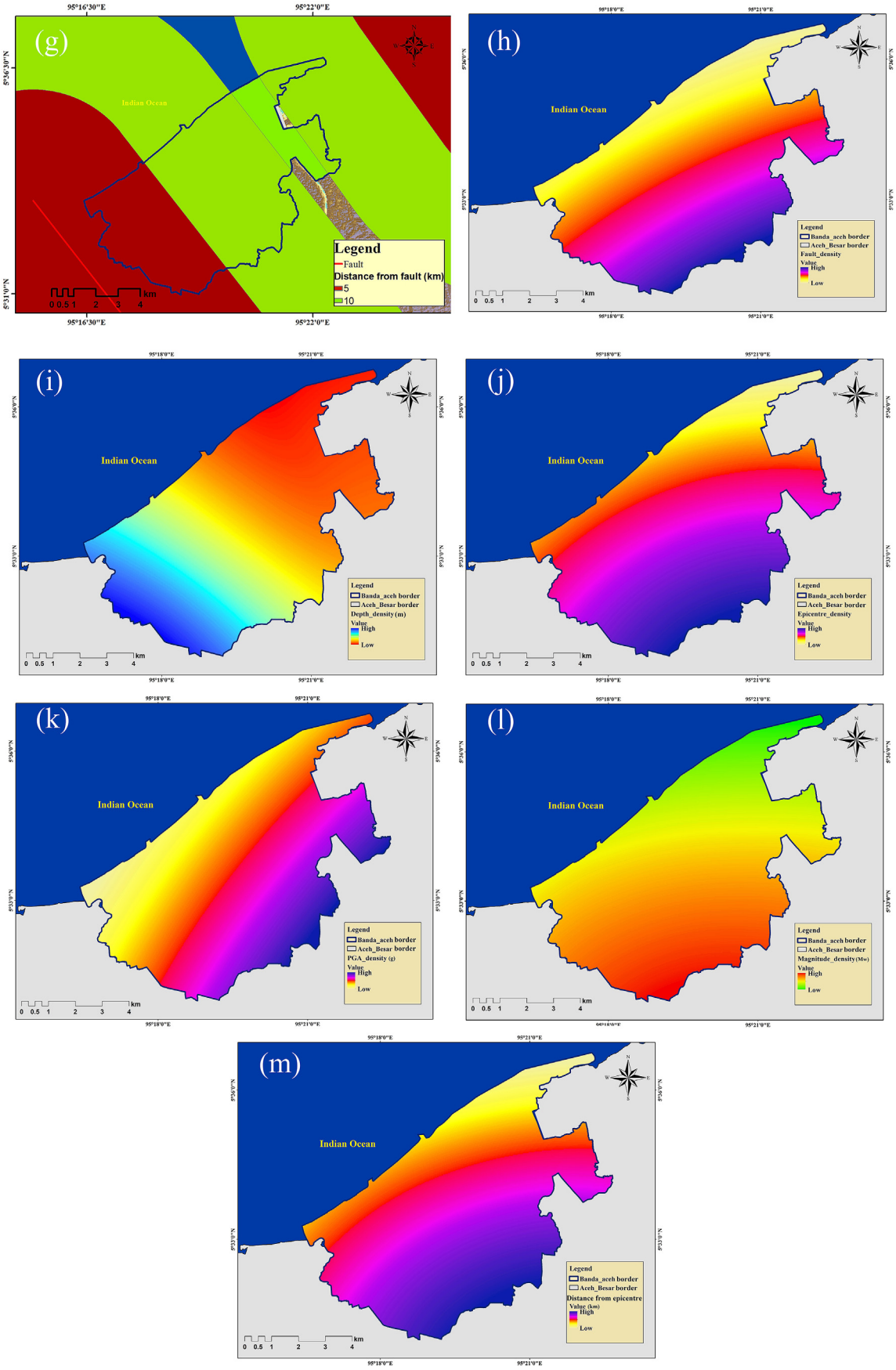

Fig. 4. (*continued*).

2005; Saaty, 2013).

5.4.1. Step 1: model construction and decision problem structuring

A problem is decomposed into a hierarchy structure that includes goal, criteria, sub-criteria, and alternatives. A relationship between the elements within an inverted tree-structured network can be specified using a suitable method (Alizadeh et al., 2018a).

5.4.2. Step 2: pairwise comparison

In AHP, the problem is described on the basis of clusters and decision elements in multiple abstractions. For example, the first cluster in this work is the goal (e.g., vulnerability mapping), the second is the criteria or the dimension, and the third is indicators (11 selected indicators are applied). A paired comparison for the decision elements was conducted in each cluster to identify the importance with respect to control criterion. Interdependencies were also inspected pairwise among the different criteria. Eigenvectors obtained from the comparison can describe the influences of elements on each other and can measure their relative significance by a scale of 1–9, in which the 1 represents equal and the 9 represents extreme significance (Panahi et al., 2014). The measurement processes through a matrix with a row component and a column component within the matrix. For reverse comparison, a correlative value was set that illustrates the (*i*th) element significance (Alizadeh et al., 2018a). The values for pairwise comparison are allocated within the matrix and computed the local priority vector that was gained from the eigenvector by the following formula (Alizadeh et al., 2018a):

$$\mathbf{AW} = l_{\max}\mathbf{W} \tag{5}$$

A is the pairwise comparison matrix and W is denoted as the eigenvector. *l*max represents the largest eigenvalue and *X* is the eigenvector of a consistency matrix (A) can be obtained by using the formula

$$(\mathbf{A} - l_{\max}\boldsymbol{I})\boldsymbol{X} = 0 \tag{6}$$

The consistency index was generally measured to define the consistency degree that can be presented using

$$\mathbf{CI} = (\boldsymbol{\lambda}_{\max} - \boldsymbol{n})/(\boldsymbol{n} - 1) \tag{7}$$

where $\boldsymbol{\lambda}_{\max}$ is the validation parameter. Consistency index (CI) is a measure of consistency of pairwise matrixes. The accepted consistency ratio (CR) value should be less than 0.1, and the equation can be represented by

$$\mathbf{CR} = \mathbf{CI}/\mathbf{RI} \tag{8}$$

The CI should be compared with RI (random index, which represents the average consistency). The ratio between them is specifically called the CI. If the estimated value is $\mathbf{CR} \leq 0.1$, then it is acceptable; otherwise, a new attempt should be repeated for the effective comparison matrix until the acceptable value is achieved.

Table 3
Parameters and stopping criteria for the ANN model.

Criteria	Parameters	Values
Input specifications	Total training points	1546
	Total earthquake events	623
Network topology	Hidden layers	2
	Hidden layer sizes	(32,64)
	Input layer nodes	13
	Output layer nodes	1
Training parameters	Activation	relu
	Solver	sgd
	Batch size	2
	Learning rate initialization	0.01
	Shuffle	True
	Random state	0
	Momentum	0.9
	Nesterovs momentum	True
	Early stopping	True
	Validation fraction	0.05
Stopping criteria	RMSE	0.3
	Accuracy rate	84

5.4.3. Step 3. calculation of supermatrix

Pairwise comparisons are applied to estimate the supermatrix that is partitioned on the basis of elements and clusters. The supermatrix characterized by *N* number of clusters is introduced in Eq. (9) (Alizadeh et al., 2018a), where Ck = kth, cluster where k= (1, 2, 3 … *n*).

The number of items are Mk in each cluster and can be presented as (ek1, ek2 …. ekmk)

W_{ij} is denoted as a priority vector. It represents the *i*th cluster significance based on cluster *j*.

$$\mathbf{W} = \begin{array}{c} \\ \mathbf{e11}\ldots\mathbf{e1m1}\ \mathbf{ek1}\ldots\mathbf{ekmk}\ \mathbf{en1}\ldots\mathbf{enmn} \\ \mathbf{C1}\ \ldots\ \mathbf{C1k}\ \ldots\ \mathbf{C1}\boldsymbol{n} \\ \mathbf{e11} \\ \mathbf{e12} \\ \vdots \\ \mathbf{e1m1} \\ \mathbf{C1}\quad \mathbf{ek1} \\ \vdots\quad\ \vdots \\ \mathbf{Ck}\quad \mathbf{ekmk} \\ \vdots \\ \mathbf{en1} \\ \boldsymbol{Cn}\quad \boldsymbol{en2} \\ \vdots \\ \boldsymbol{enmn} \end{array} \begin{bmatrix} \mathbf{Wl1}\ldots\ \mathbf{Wlk}\ldots\ \mathbf{Wl}\boldsymbol{n} \\ \vdots\quad\ \vdots\quad\ \vdots \\ \mathbf{Wk1}\ldots\mathbf{Wkk}\ldots\mathbf{Wk}\boldsymbol{n} \\ \vdots\quad\ \vdots\quad\ \vdots \\ \mathbf{W}\boldsymbol{n1}\ldots\mathbf{W}\boldsymbol{nk}\ldots\mathbf{W}\boldsymbol{nn} \end{bmatrix} \tag{9}$$

5.4.4. Step 4. selection

This step is important for assessing each indicator to choose the best one for the effective analysis and good accuracy of the result. Alternative weights can be obtained from the supermatrix in this step.

5.5. Conditioning factors

In total, 13 layers are applied for the earthquakes probability mapping. The chosen layers are based on the literature review and the trial-and-error approach in ANN (Nedic et al., 2014). Therefore, on the basis of the importance of all the conditioning factors, 13 different layers were applied, and some unnecessary layers were removed from the analysis. The ranking of layers and weights was analyzed by using ANN. The highest ranked layers were magnitude density, fault density, distance from fault, and epicenter density. These layers are followed by amplification factors, PGA density, depth density, lithology, elevation, slope, curvature, and aspect. All the layers are displayed in Fig. 4. The ANN model estimates the weight of the layers. Trial and error method helped us to understand the importance of layers and to generate the final map. Finally, the earthquake points were predicted with reasonable accuracy. The details of the parameters are explained in Table 3.

5.5.1. Environmental indicators

Lithology: Banda Aceh is characterized by quaternary sediments with patches of peridotite. Therefore, this provides an indicator of seismic amplification (Dimri et al., 2007; Alizadeh et al., 2018a). Geological formations in the study area is associated with unconsolidated sedimentary deposits, which is the main reason of ground shaking.

Slope: Slope is one of the key factors for earthquake and landslide analysis. However, slopes are associated with the faults and provide the information of fault slip (Alizadeh et al., 2018a). Slopes in the hilly drainage basins are mostly rough, where the fault size and length depends on the slope inclination (Bathrellos et al., 2017).

Elevation: This indicator is important because hilly regions are highly seismic relative to the plane lands given the complicated tectonics and structure (Alizadeh et al., 2018a). It is an important aspect of earthquake

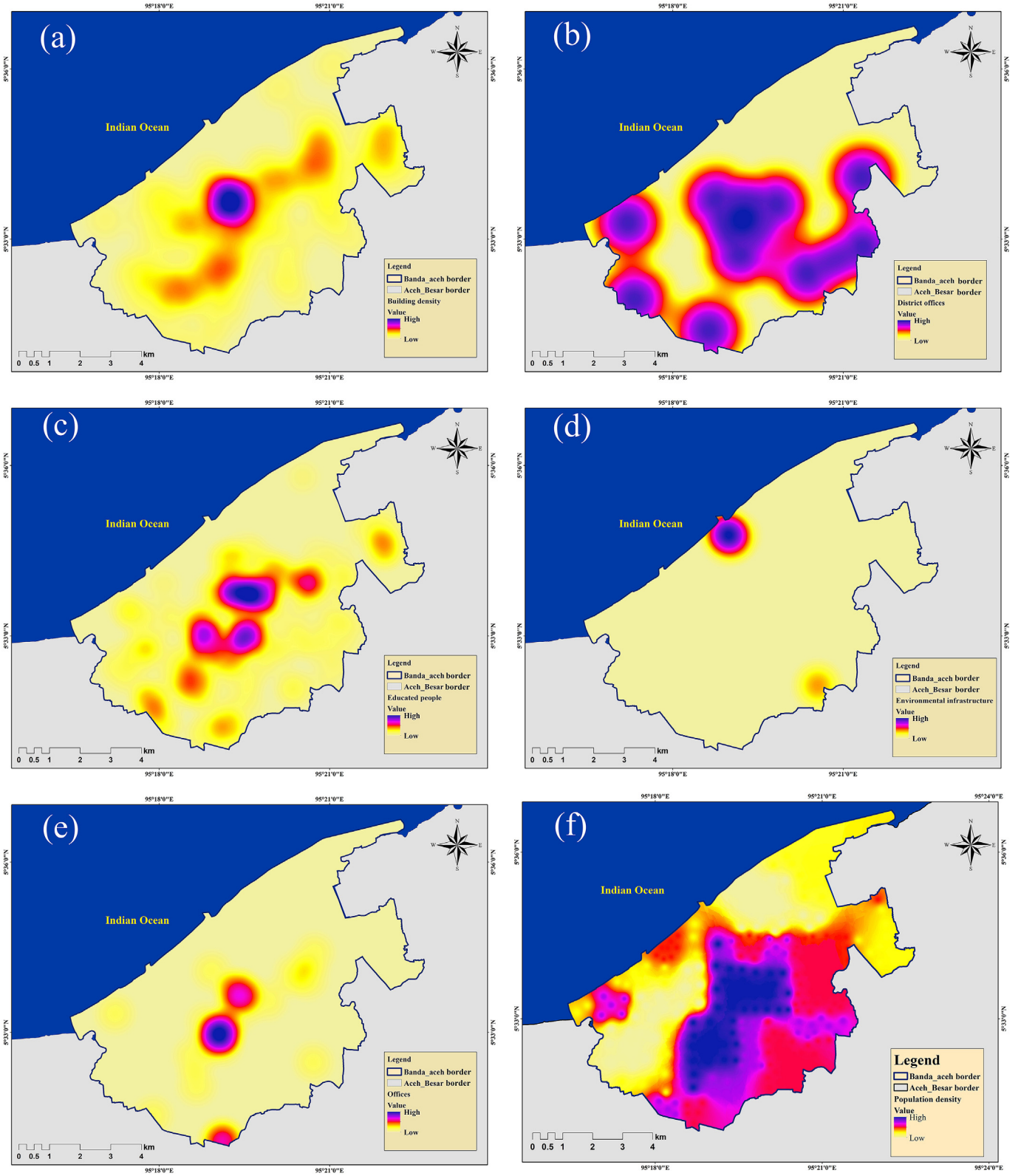

Fig. 5. Criteria for vulnerability mapping using AHP. (a) Building density, (b) district offices density, (c) density of educated people, (d) environmental infrastructure, (e) major offices, (f) population density, (g) distance from service centers, (h) stadium, (i) transportation nodes, (j) distribution universities, and (k) distribution of village chiefs.

probability mapping derived from DEM (Digital elevation model).

Curvature: It gives the positive and negative values of the surface because we can recognize the sediment deposits more in the basin than the dome part of a region, which is important for the seismic study (Gitamandalaksana, 2009).

Aspect: Generally, faults are not characterized by straight lines, plain surfaces, and those vertical to the surface. The dipping direction of faults is associated with the direction of slopes, thereby making it important for

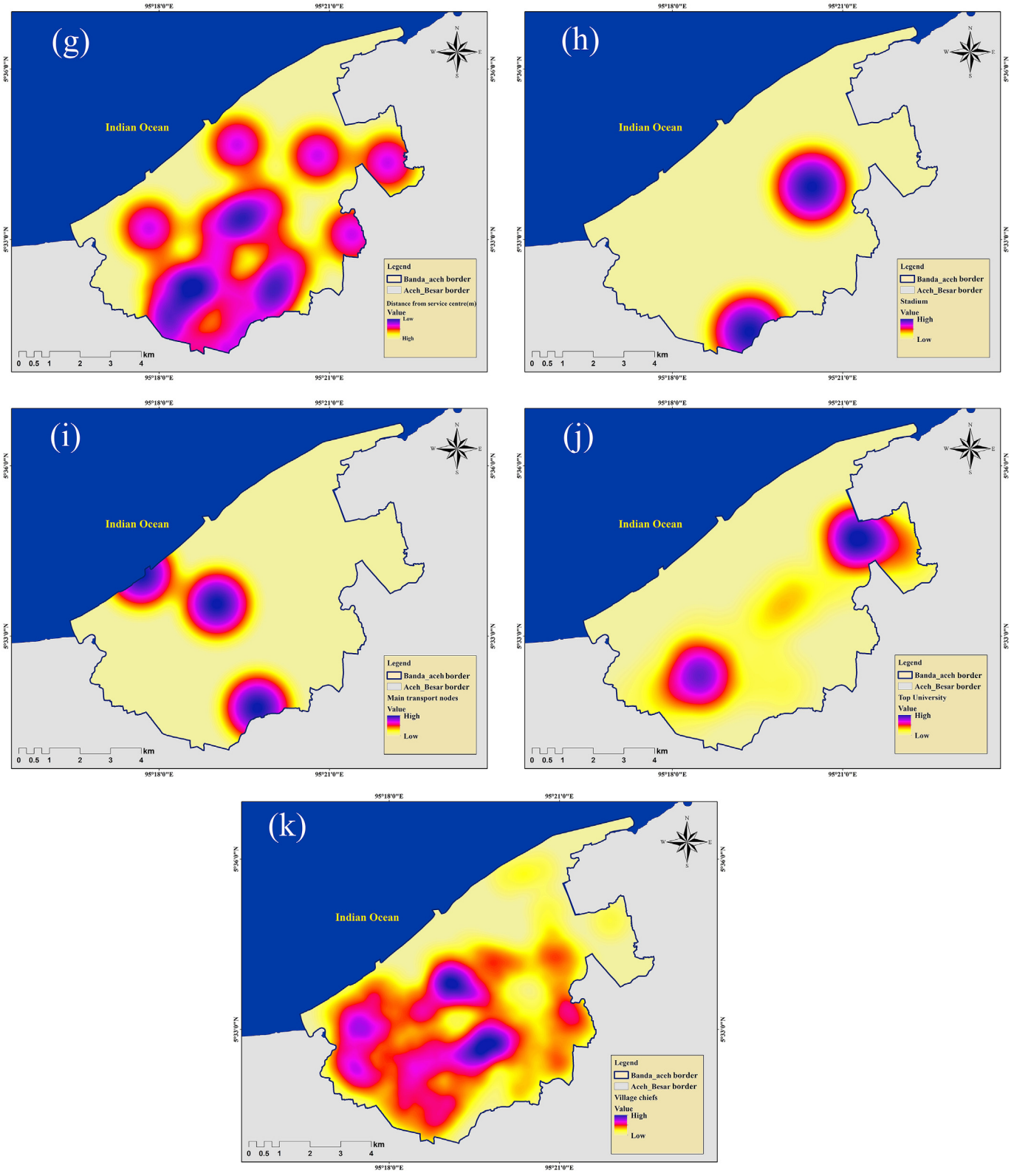

Fig. 5. (*continued*).

the study (Zebardast, 2013; Bathrellos et al., 2017).

Distance to fault: It is an important factor because the earthquake potential zones are extremely near to faults, and they decrease with distance (Martins et al., 2012; Bathrellos et al., 2017; Alizadeh et al., 2018a). All the active faults from the study area were considered in this study. Buffer zones were formulated surrounding the faults and categorized into three sections.

Fault density: Fault density is important because the high density of faults indicates the complex tectonics and are more prone areas for earthquakes (Dimri et al., 2007; Alizadeh et al., 2018a). The occurrence of earthquakes with high magnitude is associated with the fault area, therefore, the complex fault system can produce high magnitude

Table 4
Decision matrix for vulnerability assessment.

Category	1	2	3	4	5	6	7	8	9	10	11
1	1	3	0.33	3	4	2	3	5	3	0.25	2
2	0.33	1	0.25	2	3	1	0.5	1	1	0.25	1
3	3	4	1	5	5	3	3	4	3	0.5	4
4	0.33	0.5	0.2	1	1	0.33	0.33	0.5	0.25	0.2	0.5
5	0.25	0.33	0.2	1	1	0.33	0.33	0.5	0.33	0.2	0.33
6	0.5	1	0.33	3	3	1	3	3	2	0.33	2
7	0.33	2	0.33	3	3	0.33	1	3	2	0.25	2
8	0.2	1	0.25	2	2	0.33	0.33	1	1	0.2	0.33
9	0.33	1	0.33	4	3	0.5	0.5	1	1	0.25	2
10	4	4	2	5	5	3	4	5	4	1	5
11	0.5	1	0.25	2	3	0.5	0.5	3	0.5	0.2	1

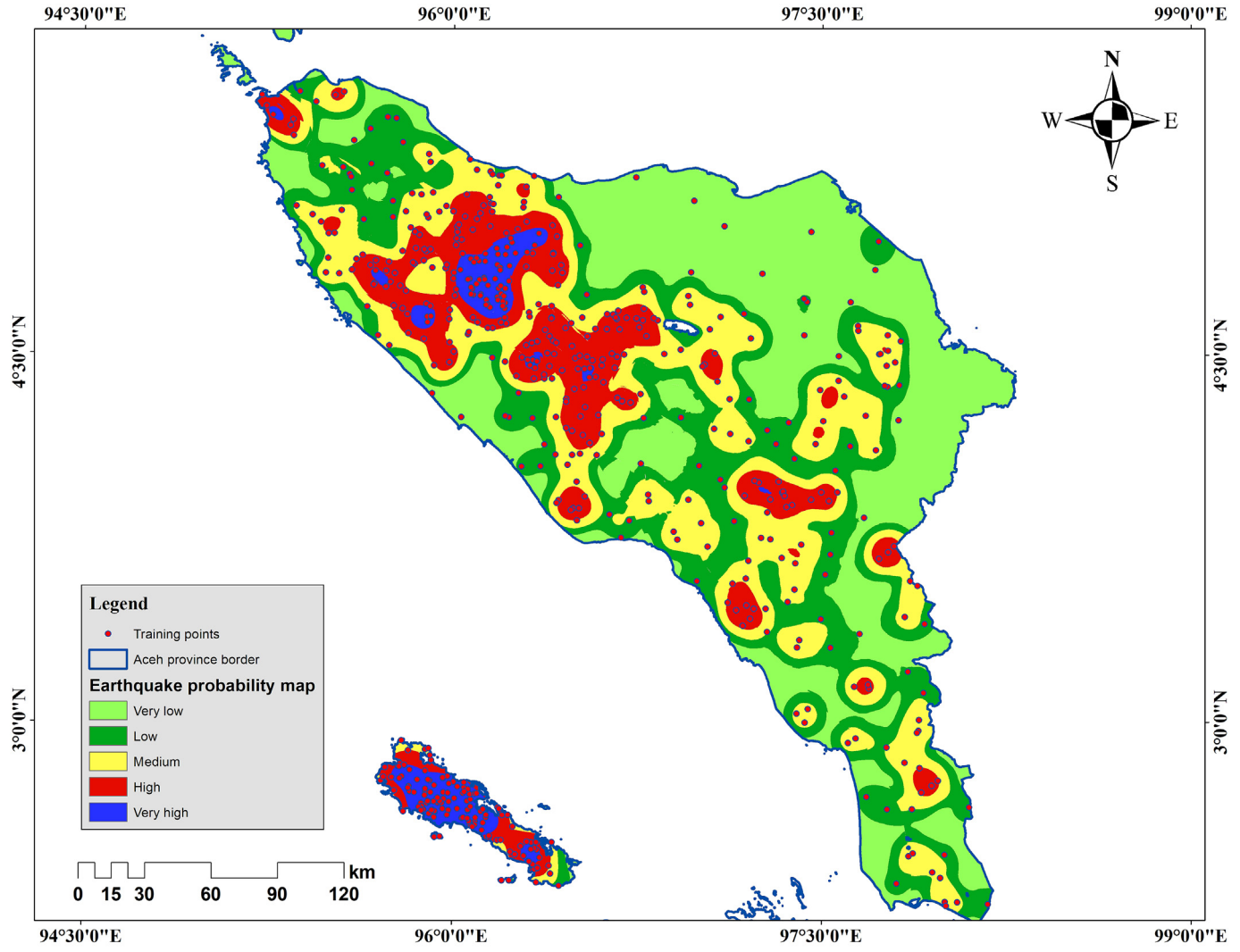

Fig. 6. Training data used for earthquake probability mapping.

earthquakes as well as in numbers (Bathrellos et al., 2017).

5.5.2. Seismic indicators

Magnitude density: Magnitude density provides the chances of occurrence of a particular magnitude of earthquake at the highly experienced zone (Soe et al., 2009; Zebardast, 2013; Bathrellos et al., 2017).

PGA density: It is an important indicator because it provides ground acceleration information that is related to the lithology, magnitude, and distance from the earthquake source zone (Soe et al., 2009; Morales-Esteban et al., 2013).

Depth density: It provides information about the fault zone if the earthquake focuses are at the same depth and the velocity of the seismic waves changes with depth, because shallow focus earthquakes are more dangerous than deep focus earthquakes (Soe et al., 2009).

Epicenter density: Epicenter density provides the zone of earthquake clustering that indicates the earthquake probable zones (Soe et al., 2009). By analyzing the epicenter density, we can focus on epicenters of a pair of large earthquakes, riftogenesis attractor structures and the main fractures (Rashed et al., 2003).

Amplification factor: It is one of the important key indicators because

the amplification value of each lithotype must be analyzed in an earthquake study (Soe et al., 2009; Morales-Esteban et al., 2013).

5.6. Vulnerability indicators

For vulnerability mapping, 11 layers were selected (Alizadeh et al., 2018a). The layers were building density, district office, educated people density, environmental infrastructure, stadium, distribution of universities, distribution of village chiefs, distance from service centers, major offices, district offices density, population density, and transport nodes, as presented in Fig. 5. For pairwise comparison, the relative importance of the layers was estimated on the basis of Table 4. Then, by applying the normalization technique, the weight and rank of all the layers were evaluated. In the next step, the weighted sum tool in the GIS is used to make the vulnerability map.

5.6.1. Social indicators

Population density: The population density is increasing every year, as indicated by the 2000–2017 census data. Unfortunately, the increased population density is towards the seismic gap of the GSF fault in Banda Aceh, thereby resulting in high vulnerability (Rygel et al., 2006; D'Ayala et al., 2008; Armaş et al., 2012; Alizadeh et al., 2018a). We did not consider the age, male, female indicators in this study because of inaccessible data.

Educated people density: A higher level of literacy can increase more about the awareness of hazard among the people than uneducated people. Education can enhance responsibilities during disasters (Rygel et al., 2006; Alizadeh et al., 2018a). These are 2nd level of factors after the population density which is directly associated with vulnerability assessment (Martins et al., 2012).

University distribution: Universities are the main source of education that can raise crisis alarms hazards. Therefore, the good distribution of universities in a large city is significant (Alizadeh et al., 2018a). This is the indicator in which the condition of total availability of students, daytime and nighttime vulnerability indicators were not considered (Martins et al., 2012).

Village chief distribution: "Chiefs" are the highly respected persons in village areas. Through chiefs, the government can provide information on disasters to the people (Armaş et al., 2012; Alizadeh et al., 2018a).

5.6.2. Physical indicators

Building density: Land allocation, lowering building construction, and equal distribution of buildings, along with a perfect development plan, can decrease vulnerability to disasters (Aghataher et al., 2008; Alizadeh et al., 2018a). Having an aim to minimize future destruction may associate with future seismic activity, it is important to focus on buildings to reinforce the old structures in the city, which are vulnerable (Oliveira et al., 2003).

Service centers and offices: The main offices and the service center distribution is extremely important for a well-planned city in lowering vulnerability (Alizadeh et al., 2018a).

Transportation nodes: Transportation nodes are a key factor in disaster management. Street classification is more important than system performance (Rashed et al., 2003; Alizadeh et al., 2018a).

Environmental infrastructure: It is one of the major factors that must be considered for earthquake vulnerability assessment (Wisner et al., 2003). Environmental infrastructures need to be updated to reduce the vulnerability (Alizadeh et al., 2018a).

Stadiums: Stadiums full of people are more vulnerable than empty stadiums (Rygel et al., 2006).

5.7. Implementation of developed model

In this current analysis, an ANN–AHP model was developed and implemented as follows. A feed-forward ANN with a three-layered structure was applied, and we trained the large area of Aceh province with a set of earthquake data points and an applied backpropagation algorithm for root mean square error (RMSE) calculation. Feed-forward ANN clearly describes the interconnection between the neurons in different layers. Then, the small area of Banda Aceh was applied to test and to map the probability. First, the input data layers were converted into multiple data point values. We load some external libraries to conduct modeling in the first step; these libraries include operation system, data management, numerical analysis, and neural network. We also performed this step to measure the error rate of a model and for plotting purposes. In the next step, we built a neural network using the MLP classifiers. Then, we applied normalization to all the layers. In the next step, we trained the neural network for probability mapping. We measured the accuracy of the trained model. Then, we predicted the pixel values for the study area of Banda Aceh. The final map of probability was the result, which we analyzed on the basis of the literature review and expert experience. The final probability map was characterized with high to low probability of earthquake occurrence in Banda Aceh. Consequently, we produced a hazard map by considering the earthquake intensity distribution. Then, we classified the hazard map into five different zones. The ANN model works significantly with good accuracy. The AHP methodology was implemented for vulnerability mapping based on the steps described above in AHP methodology architecture. Layers for analysis were chosen correctly and referred to some current literature. In addition, the quality of the results was analyzed on the basis of the achieved CR (0.04), which yielded good results. Finally, we multiply both the hazard and vulnerability map to produce the earthquake risk map.

5.8. Performance evaluation

This section is important for understanding the obtained results. Several metrics are available that are used as benchmarks to analyze the performance of our projected neural network model, such as space, time, and model accuracy. Although time and space are highly important for the training of a model and may create an obstacle; therefore, we applied RMSE to evaluate the performance of applied ANN inside the ANN–AHP model. Several researchers have applied and understood the best performance obtained by the metric RMSE, which was selected on the basis of problem nature and the expected results (Alarifi et al., 2012). The results of our ANN model and AHP method are presented in the section of results and discussion. The presented results are easy to understand and facilitate decision-making.

5.9. Performance metrics

5.9.1. Mean absolute error (MAE)

MAE is a quantity used to measure how close predictions are to the target outcomes. The mean absolute error is defined as follows:

$$\mathbf{MAE} = 1/\boldsymbol{n}\sum_{i=1}^{n}|\boldsymbol{error}_i| \tag{10}$$

5.9.2. Root mean square error (RMSE)

RMSE estimates the average error based on a quadratic scoring rule. RMSE is the square root of the average of squared differences between prediction and actual observation. It provides the average prediction error of a network. The values of RMSE ranges from zero to infinity. However, the lower values expressed by the RMSE gives a better result. RMSE is better than the mean absolute error (MAE), whereas large errors are unacceptable. Therefore, RMSE is more appropriate for error measurement (Alarifi et al., 2012).

$$\mathbf{RMSE} = \sqrt{1/\boldsymbol{n}\sum_{j=1}^{n}\left(y_j - \widehat{y_j}\right)^2} \tag{11}$$

The RMSE values $\widehat{y_j}$ that are predicted for times j of a variable of

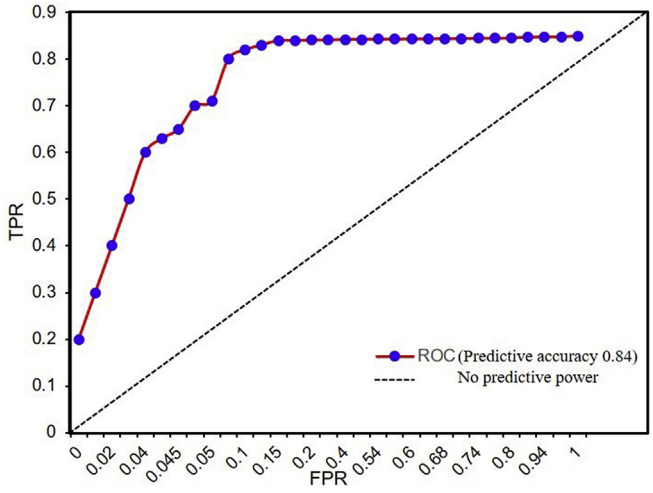

Fig. 7. Accuracy assessment curve (ROC) for the earthquake probability map.

Table 5
Prediction results using ANN.

False positive rate (FPR)	True positive rate (TPR)	1-FPR	TF	Thresholds	Crossover
0.132982	0.848876	0.867018	−0.048142	1	1

Total earthquakes belong to predicted pixels: 616 earthquakes out of 1546 training points of Aceh province.
The Total Area Under Risk: 608,400 m^2 in the Aceh province.

regression's dependent y_j with y different predictions for observed variables over T times is computed as the RMSE. The RMSE value for this study is 0.3 based on the training site of Aceh province with an accuracy value of 0.84. An accuracy curve (ROC) was developed and described in the results and discussion part of the paper.

6. Results and discussion

6.1. Probability and hazard results of applied MLP

6.1.1. Probability estimation

MLP calculates the information based on the training data. MLP executes the analysis of a non-parametric regression between the input and dependent variables finally in the system that were recognized by an output neuron. MLP was applied to map the earthquake probability in Banda Aceh. The probability results indicate that the training accuracy was reasonably good with a total prediction of 616 earthquake points out of 624. The approach was unable to predict the other eight earthquakes because of the noise in the probability indicators.

The total prediction was out of 1546 training points characterized by both earthquake and non-earthquake points in Aceh province, as presented in Fig. 6. The total area predicted from the network under risk is approximately 608,400 m^2 in Aceh province. Then, the model tested for the study area of Banda Aceh as the capital of Aceh province. The true positive rate (TPR) and false positive rate (FPR) that was obtained the Banda Aceh were 0.84 and 0.13, respectively. The rate of 0.13 shows that each time we call for a positive, we obtain this specific probability of being wrong. Therefore, this value is called the false positive rate. Likewise, a true negative rate can be analyzed. The graphical representation of accuracy is presented in Fig. 7.

The details of TPR, FPR, 1-FPR, TF, threshold, and crossover are listed in Table 5. The accuracy of the prediction was 0.84 with RMSE 0.3. Given that the city is very small and is located near the GSF with no evidence of historical earthquakes, the seismic gap in Aceh province may experience future earthquakes. However, the high probability areas can be found in the SE corner of the city, and low probability can be found towards the NW corner of the city as per the resultant probability map. The map explains the potential zone for earthquakes within the city, as presented in Fig. 8. The SE region of the city found to have very high probability, whereas the NW part of the city falls under very low probability. The reason behind the high probability in this region is the high fault density, epicenter density, magnitude density, and low distance from the active fault along with high height and amplification value as the city is mostly covered with quaternary sedimentary rocks. The low probability of the NW part of the city is because of low epicenter, magnitude, and active fault density, along with low height and slope.

6.1.2. Hazard estimation

A hazard map was developed using the probability map and presented in Fig. 9. The main objective of the hazard map is to provide information on the extent of possible damage and the activities of disaster prevention. The most important point is to provide residents with comprehensible information by hazard map. The level of danger of an earthquake can be understood by its intensity. The intensity pattern in the study area can be defined on the basis of the historical records of destructive earthquakes and statistical calculations. Near Banda Aceh along the GSF, high-intensity earthquakes may occur occasionally. We calculated how high the level of destruction can be in case of such high-intensity earthquakes. Therefore, we assumed that when the earthquake intensity becomes more than 9, the hazard will be very high, whereas the intensity 8–9 will be considered high hazard areas, 8–7 is considered medium, 7–5 is low, and below 5 is very low. The hazard map was classified into five different classes based on the quantile classification technique. The results indicate that very high hazard can be found in the SE part of the city and very low hazard in the NW part because of high magnitude earthquakes near the SE part of the city. This type of hazard map is the basic map for the administrative agencies that can be used for disaster prevention services. These maps are used to develop an evacuation and warning system, as well as available facts for land use regulations. These maps can also be used in inhibitory works.

For the results described in this section, we recognized that the better capabilities of a neural network for earthquake prediction and probability modeling characterized by nonlinear and complex relationships among the variables is a developed model to handle variable interactions. Neural networks are not an easily understandable model, but they become complicated with a large number of variables. The performance results explained in this study indicate that the potential of a neural network can be useful for earthquake probability mapping in other study areas and is worthy of further investigation.

6.2. Vulnerability index estimation

Integration and aggregation of the various significant indicators described in the data table are included in the tree of the AHP approach. Table 6 shows the process and the criteria weights in the hierarchical tree. The calculated rank of criteria, as well as the eigenvalues and consistency ratios, are presented in Table 6. The experts can understand the resulted weights and ranks for various criteria by the preliminary investigations, and they can monitor the AHP approach adaptation and review the obtained vulnerability map and the associated uncertainties, thereby approving the resulting map. We considered all the layers, analyzed the significance of all the layers using the AHP ranking approach, and applied them to GIS for the vulnerability mapping.

The resultant vulnerability map (Fig. 10) was acquired by the processing of several vulnerable indicators. In total, 55 comparisons were made with the resultant CR of 0.04. The principal eigenvalue was 11.728 based on the analysis, and the eigenvector solution was five iterations.

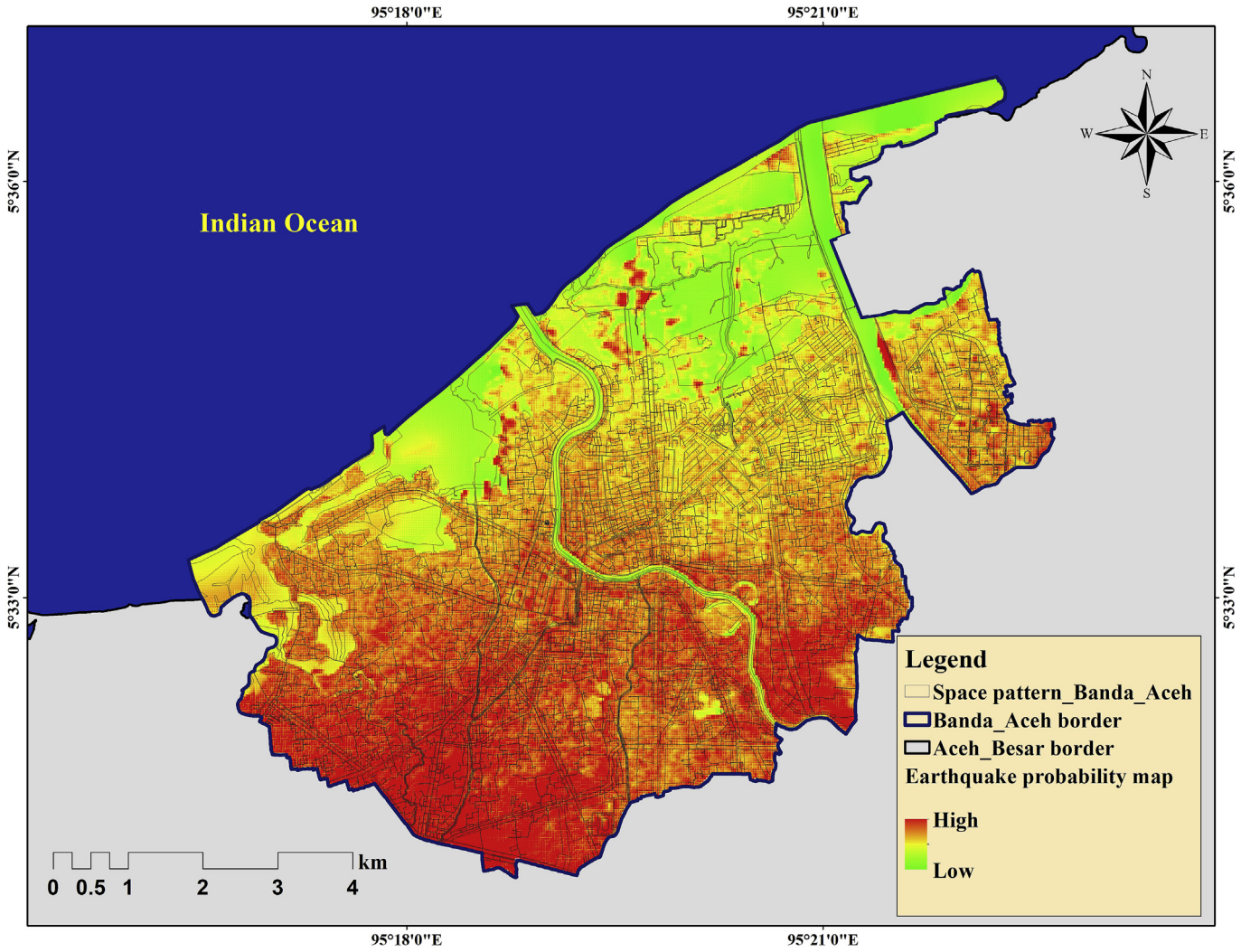

Fig. 8. Earthquake probability map.

Mathematically, an eigenvalue that should be non-zero, which corresponds to an eigenvector, points in a direction that is stretched by the transformation. The eigenvalue is the factor by which it is stretched. A negative eigenvalue represents a reverse direction. However, the CR shows that the importance of all the layers is evaluated carefully and accurately. The delta value of 3.3E−8 was obtained from AHP in this analysis. Population density, educated people, and building density were ranked as 1, 2, and 3, with weights of 24.9%, 19.2%, and 12.2%, respectively. The lowest rank was obtained by environmental infrastructure and stadium, whereas the remainder were ranked medium. The resultant map was classified into five different categories according to experience: very low, low, medium, high, and very high. The results indicate that the mapped areas can be calculated using the option of geometry. Very high vulnerability can be found in the south-central part of the study area because of the high building and population density, along with the government offices and educated people density. Very low vulnerability was observed in the NW part because of the reverse conditions in the region. Therefore, our map is good and useful for national and local government organizations in their vulnerability mapping.

6.3. Risk estimation

An earthquake risk map was prepared for Banda Aceh by multiplying the hazard and vulnerability map. The resultant map was classified into five classes by using the quantile classification technique (Birkmann and Welle, 2015). Therefore, the areas of all the classes were calculated for the city and for different zones within the city. The geometry showed that 7.23% of the entire area was under extreme risk. High, moderate, low, and very low-risk zones represent 15.31%, 20.99%, 28.70%, and 27.72% of the total area, respectively (Table 8). On the basis of the geographic position, the east-southern part of the city, comprising zones 2, 3, 5, 6, and 7, represent the regions with moderate risk. Given the few people and low infrastructure in the zones, 1, 4, 9, and some parts of 3 and 8, the risk chances are low. However, in the south to central regions of the city, zones 3, 5, 7, 8, and some parts of 6 are considered high-risk areas because of the high population density, building density, educated people, government offices, and proximity to the seismic gap of GSF.

By simply understanding the vulnerable and hazard zone size and area, one can obtain the impact level of the probable future earthquakes. Therefore, population data of Banda Aceh were used for estimation of the population risk. Thus, risk mapping was conducted in all nine zones of Banda Aceh, as illustrated in Fig. 11 and graphically presented in Fig. 12.

The most clustered risk zones are identified. Overall, three zones are considered highly risky areas; the main reason is their geographical location and high population. The detailed calculations of earthquake population risk and area risk for nine different zones and for the entire area are presented in Tables 7 and 8, respectively.

The issues can be understood by considering five main situations.

(1) Areas with very high population, structural, and geotechnical vulnerability comprise 7.23% risk area of the total area. The most at-risk zones are located, as per the results, in zones 3, 5, and 7;

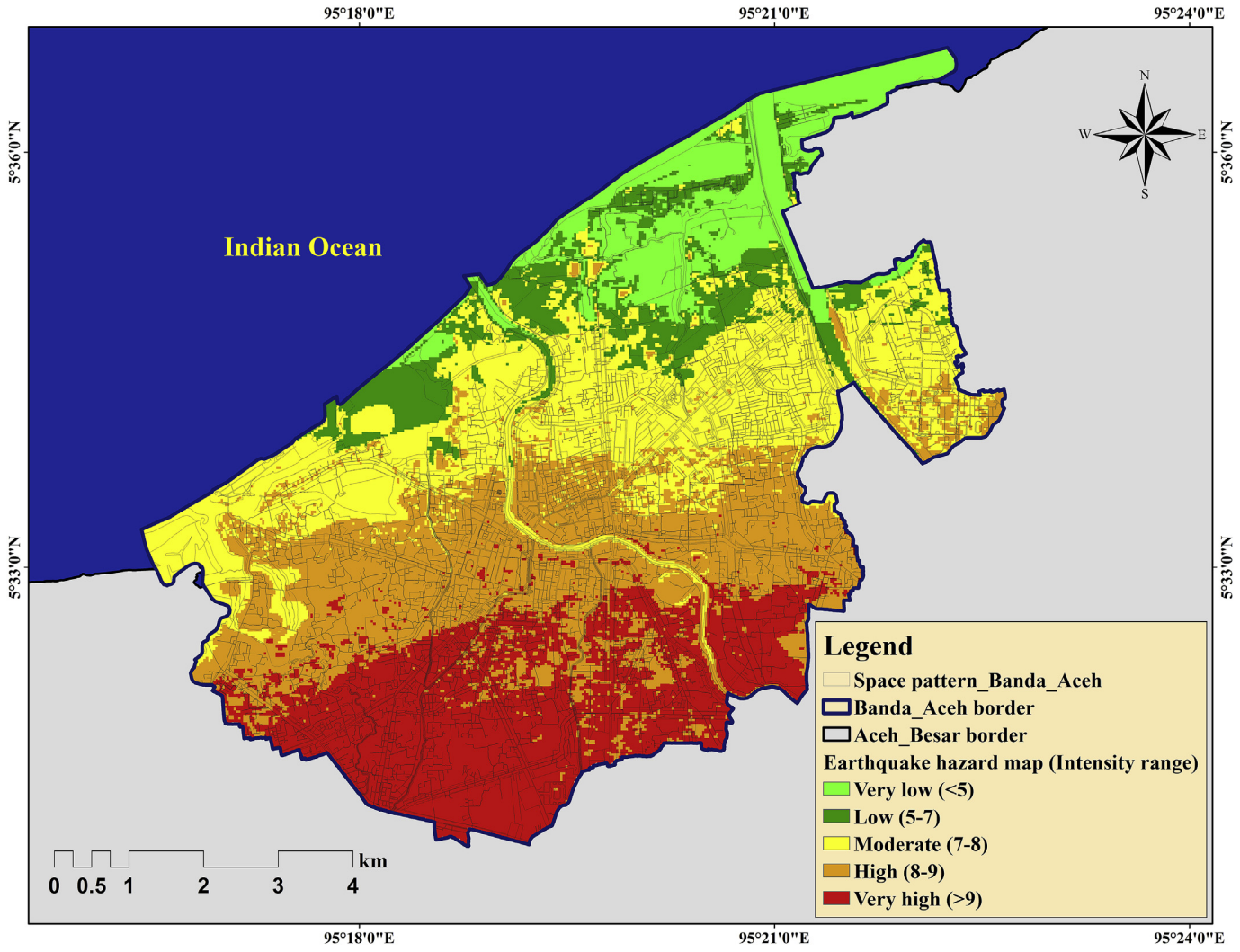

Fig. 9. Earthquake hazard map.

Table 6
Evaluation of weights and rank of layers.

Category	Name	Priority	Rank
1	Building density	12.8%	3
2	District office	5.3%	8
3	Educated people density	19.2%	2
4	Environmental infrastructure	2.8%	10
5	Stadium	2.6%	11
6	Distribution of universities	9.3%	4
7	Distribution of Chiefs	7.6%	5
8	Distance from service centers	3.9%	9
9	Major offices	6.0%	6
10	Population density	24.9%	1
11	Transport nodes	5.4%	7
	Number of comparisons = 55		
	Consistency Ratio CR = 0.04		
	Principal Eigen value = 11.728		
	Eigenvector solution: 5 iterations		
	delta = 3.3E-8		

either demolition or reconstruction of poor quality buildings are required.

(2) The highest number of buildings can be found in the central part of Banda Aceh. However, buildings are situated in zones 2, 3, 5, 7 and 8, and their risk can be reduced by retrofitting and modification based on seismic ground shaking.

(3) Moderate risk from geotechnical, structural, and social indicators is found in nearly 20.99% of the city area. Populations in zones 1, 2, 6 and some parts of zones 3, 5, 7 are under moderate risk. Retrofitting or, occasionally, destruction or renovation of the buildings can reduce risk.

(4) Populations with low risk can be found in 28.70% of the city. The buildings in zones 1, 2, 6, 8, and 9 are safe and not particularly vulnerable.

(5) An extremely low density of residential buildings with low population, which showed very low risk, comprise approximately 27.72% of the total area. By considering the circumstances of structural and geotechnical data, the buildings in this area are under less risk than those in other classes.

7. Validation

Validation of the resulted probability map was implemented in sequence to examine the accuracy (Mohammady et al., 2012; Zare et al., 2013; Pradhan et al., 2014; Tehrany et al., 2014; Youssef et al., 2015; Aghdam et al., 2016; Tien Bui et al., 2016; Fanos and Pradhan, 2019) in Fig. 13. The trained model of Aceh province was obtained and converted to a probability map of Aceh using GIS. The trained earthquake probability map was presented with five different classes to recognize various

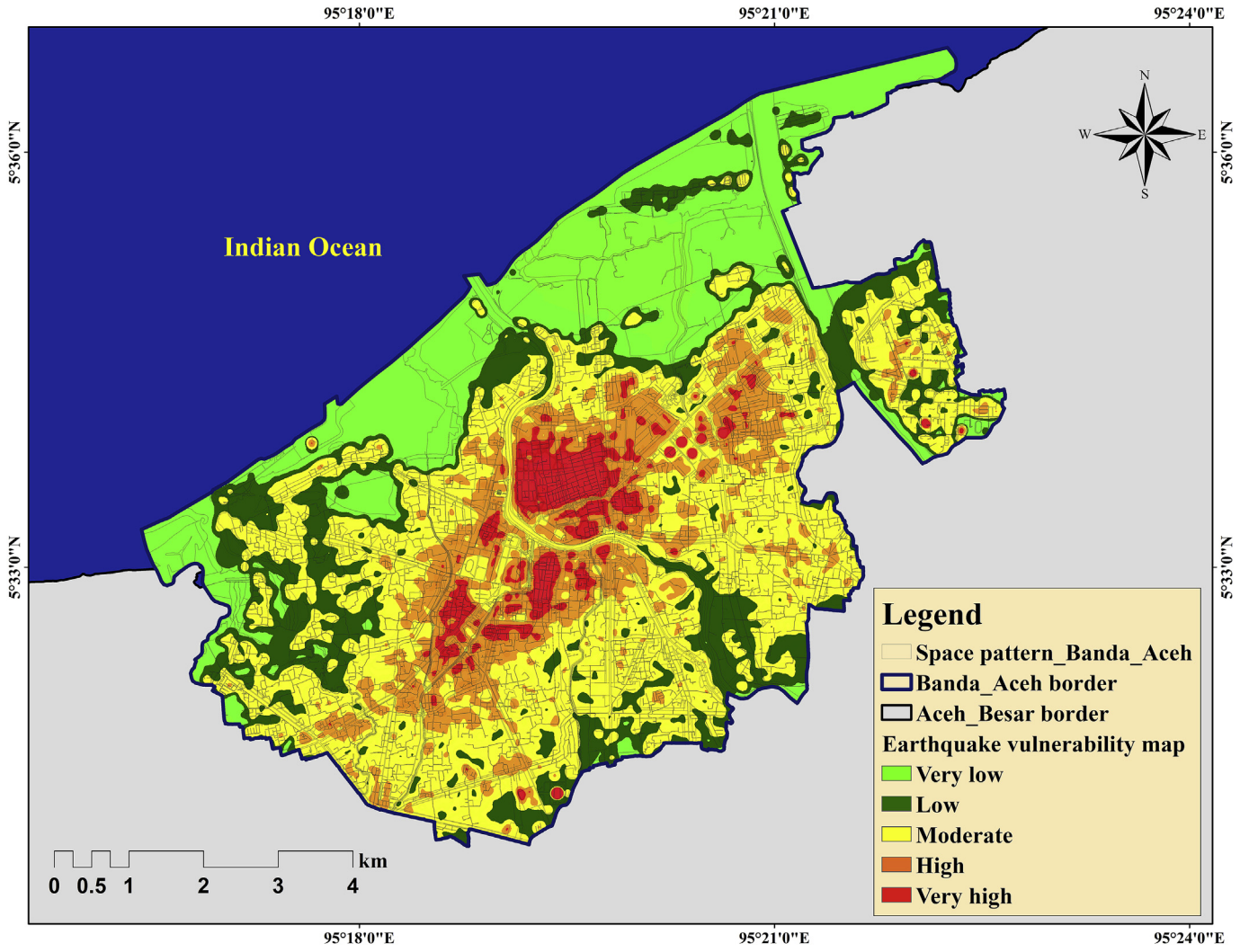

Fig. 10. Earthquake vulnerability map.

zones of probability, as previously shown in Fig. 6. A well-constructed map accurately shows the domain of interest. If we consider the location of Banda Aceh in the trained map of probability, then we can understand that the result of Banda Aceh matched with the trained map. Not achieving such accuracy may occur when using standardized/classified data. The total number of training points of earthquakes and the surrounding earthquakes of Aceh province were also used to validate the result. Mostly, the earthquakes were focused on the east, west, and southern regions of Banda Aceh. Therefore, we find that the resultant probability map has a high probability of earthquake occurrence towards the east, west, and southern regions. The histogram of earthquake probability was also presented to understand the flow of probability from one part of a city to the other parts. Hence, the domain mentioned here in this study can be notably seen in the output that represents compatibility and flexibility, proven with a human perspective. To validate the model results of integrated ANN–AHP following the literature review, historical earthquake probability mapping results, historical events, and earthquake impacts must be considered. However, on the basis of the model accuracy of ANN and the CR of AHP, our proposed result is significantly good.

8. Conclusions

In this study, we developed a model for the earthquake risk estimation in an urban area using an integrated technique of ANN–AHP. The model is a GIS-based spatial analysis useful for the city scale. The adopting information about the indicators selection from the literature with combined techniques was advantageous and effective for ERA that was applied for Banda Aceh. However, the incorporation of knowledge about geomorphology, geology, and structural information, as well as the data of historical earthquake events, are important and will aid in generating an earthquake risk map for the city. Nine zones of Banda Aceh were used into the investigation as two groups of analysis characterized by several sub-parameters.

The ANN model is extremely useful for earthquake probability measurement, and the AHP method is useful for the weight calculation of the parameters for earthquake vulnerability assessment. The ranks and weights were decided on the basis of the judgments and preferences of the authors. Given that the RMSE is very low, the ANN model has a low chance of misinterpretation of the earthquake probable areas, and the CR in AHP shows the quality of vulnerability results. The developed method found that an urban area may have several risk patterns if all factors are considered. Findings indicate that the geological factors have contributed the highest impact to earthquake probability assessment, whereas social factors contribute highest for vulnerability assessment in Banda Aceh. However, factors vary in different zones of Banda Aceh. The results reveal that the highest risk zones were possibly 3, 5, 7, and 8 in the central-southern part of the city. Comparatively, the other parts have low-to-moderate earthquake risk. Developmental infrastructure and master plans of the city show that it is expanding towards the southern

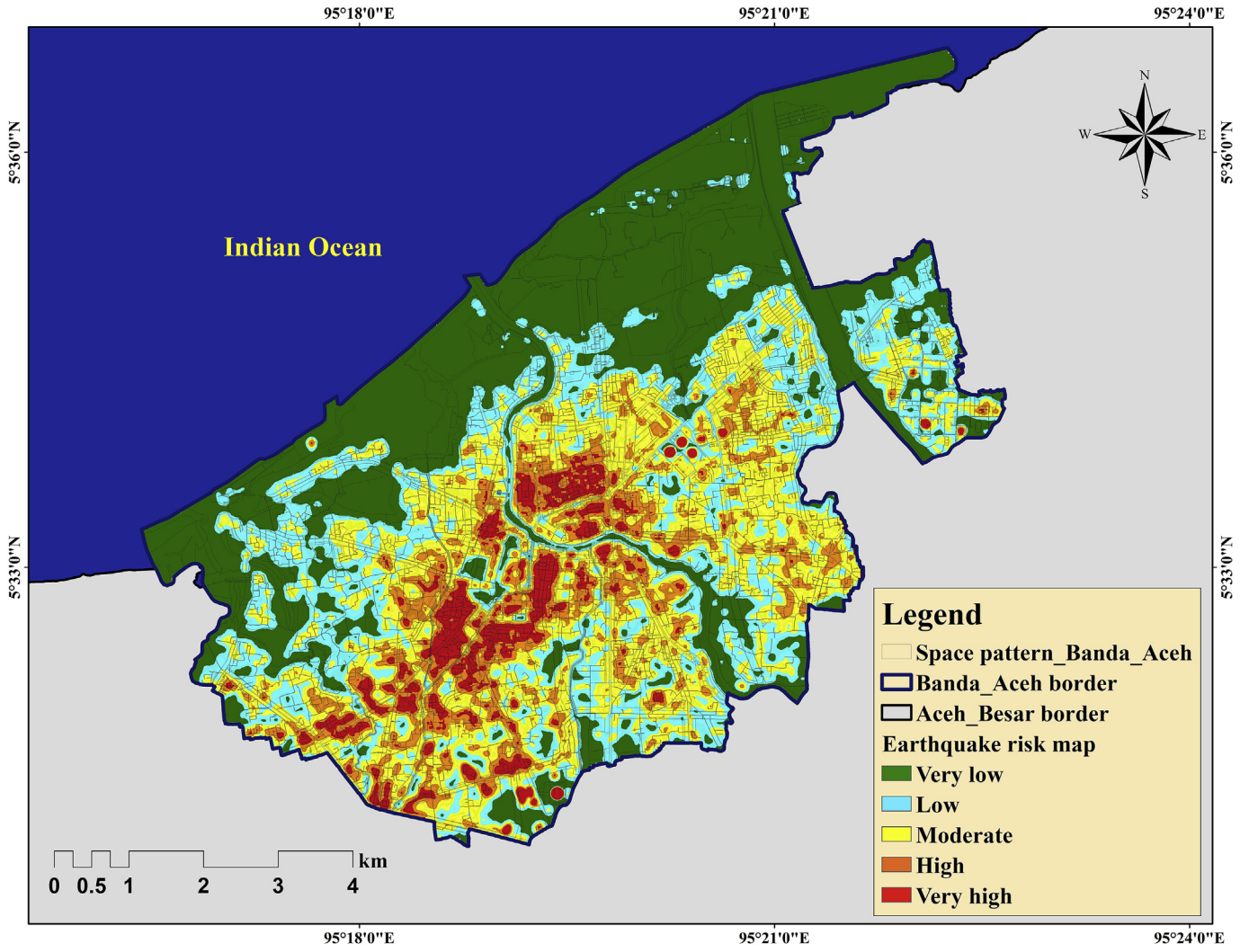

Fig. 11. Earthquake risk map.

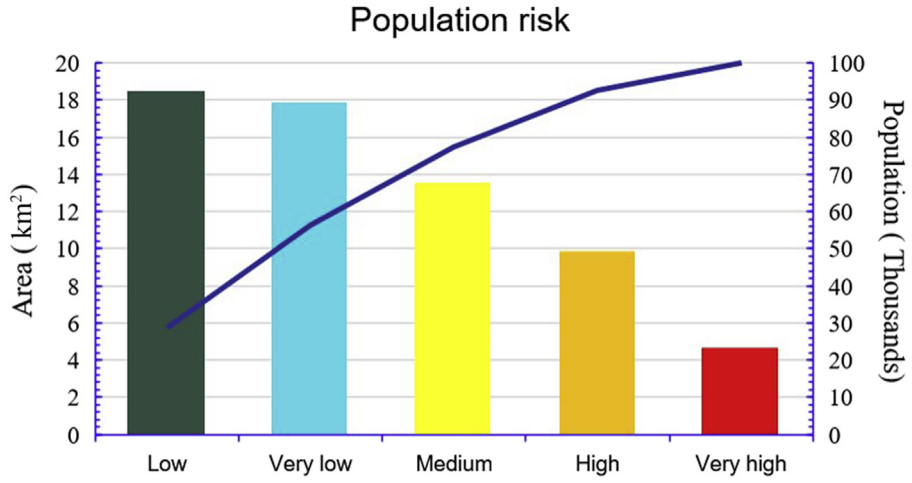

Fig. 12. Estimated number of population and area within the risk zones.

direction towards the GSF fault. Thus, at present, parts of the city with various schools, universities, and informal settlements are situated near the fault. Settlements, construction, and a developmental city plan near the fault may cause a serious problem in future if the city grows towards the fault without attention being placed on dangers posed by faults and many other concerns.

Population density and building density are high in the very high-risk zones. Government offices and the main transportation junctions can critically exacerbate the conditions. The city deserves outstanding consideration of support from the local and the national government to

Table 7
Estimated earthquake population risk and area.

ID	Risk	Area (km^2)	Hectare	Percentage	Population in risk
1	Very low	17.894	1789.46	27.72	65167
2	Low	17.524	1752.40	28.70	76268
3	Medium	12.55	1255.80	20.99	47981
4	High	9.885	988.56	15.31	32363
5	Very high	4.669	466.92	7.23	14018
Total		62.53	6253.14	100	235,797

reassess the managing strategies of natural disasters because the city already was exposed to the 2004 tsunami and its consequences. Therefore, appropriate guides are needed to manage the city and aid decision-makers to recognize the influence of various factors and to understand the deficiencies in each zone. The critical condition of buildings and the populated risk zone area should be included in government observations, and programs of risk reduction must be improved. Lack of proper space distribution within the city and poor developmental city planning can be considered the future factors for risk. Therefore, the ANN–AHP model in this study provides an effective

Table 8
Estimation of earthquake risk area and population under risk in nine zones of Banda Aceh.

ID	Risk	Area (km^2)	Hectare	Percentage	Zone	Name
2	Low	4.764	476.4	32.89		
1	Very low	8.962	896.2	61.88		Syiah Kuala
3	Medium	0.735	73.5	5.075	1	
4	High	0.022	2.2	0.15		
			1448.3	**100**		
3	Medium	2.73	281.9	55.6		
2	Low	2.2	220	43.4	2	Ulee Kereng
4	High	0.05	5	0.99		
			506.9	**100**		
1	Low	1.981	198.1	21.2		
2	Very low	3.365	336.5	36.024		
3	Medium	1.923	192.3	20.586	3	Kuta Alam
4	High	1.092	109.2	11.69		
5	Very high	0.98	98	10.49		
			934.1	**100**		
1	Very low	1.347	134.7	37.89		
2	Low	1.436	143.6	40.39		
3	Medium	0.582	58.2	16.37	4	Kutaraja
4	High	0.179	17.9	5.035		
5	Very high	0.011	1.1	0.309		
			355.5	**100**		
4	High	2.5	250	22.32		
5	Very high	2.53	253	22.7		
3	Medium	1.53	153	8.27	5	Baiturrahman
2	Low	1.1	110	45.8		
			766	**100**		
2	Low	1.771	177.1	27.75		
3	Medium	1.939	193.9	30.38		
4	High	2.487	248.3	38.906	6	Lueng Bats
5	Very High	0.189	18.9	2.96		
			638.2	**100**		
2	Low	0.592	59.2	12.82		
4	High	2.145	214.5	46.63		
3	Medium	1.599	159.9	34.76	7	Banda Raya
5	Very high	0.264	26.4	5.74		
			460	**100**		
3	Medium	1.24	124.83	26.71		
4	High	1.26	126.27	27.024		
5	Very high	0.66	66.95	14.32	8	Jaya Baru
2	Low	1.3	130.94	28.023		

ID	Risk	Area (km^2)	Population in risk	Percentage	Zone	Name
2	Low	3.38	12309	39		
1	Very low	4.04	14713	45.5		
3	Medium	1.27	4625	14.44	9	Meuraxa
4	High	0.15	546	1.754		
5	Very high	0.035	127	0.45		
			32322	**100**		
3	Medium	1.24	5837	37.41		
4	High	1.26	4588	27.024		
5	Very high	0.66	1082	3.627	8	Jaya Baru
2	Low	1.3	4734	28.023		
1	Very low	0.18	655	3.907		
			16898	**100**		
5	Very high	0.592	2156	11.843		
4	High	2.645	9633	52.91		
3	Medium	1.499	5459	29.97	7	Banda Raya
2	Low	0.264	961	5.27		
			18210	**100**		
2	Low	1.771	7449	32.14		
3	Medium	1.939	8061	34.79		
4	High	2.487	6966	30.06	6	Lueng Bats
5	Very high	0.189	694	2.99		
			23170	**100**		
4	High	2.53	6292	22.75		
5	Very high	2.5	6351	22.96		
3	Medium	1.53	2295	8.3	5	Baiturrahman
2	Low	1.1	12710	45.97		
			27648	**100**		
1	Very low	1.347	4906	37.89		
2	Low	1.436	5230	40.39		
3	Medium	0.582	2119	16.37	4	Kutaraja
4	High	0.179	652	5.035		
5	Very high	0.011	40	0.309		
			12947	**100**		
1	Low	1.981	7214	21.2		
2	Very low	3.365	12255	36.024		
3	Medium	1.923	7003	20.586	3	Kuta Alam
4	High	1.092	3977	11.69		
5	Very high	0.98	3569	10.49		
			34019	**100**		

(*continued on next page*)

Table 8 (*continued*)

ID	Risk	Area (km^2)	Hectare	Percentage	Zone	Name
1	Very low	0.18	18.26	3.907		
			467.25	**100**		
1	Low	3.38	338.42	38.06		
2	Very low	4.04	404.14	45.45		
3	Medium	1.27	127.57	14.34	9	Meuraxa
4	High	0.15	15.46	1.74		
5	Very high	0.035	3.525	0.4		
			889.115	**100**		

ID	Risk	Area (km^2)	Population in risk	Percentage	Zone	Name
3	Medium	2.72	9906	53.66		
2	Low	2.2	8312	45.02	2	Ulee Kereng
4	High	0.05	242	1.31		
			18460	**100**		
2	Low	4.764	17350	32.89		
1	Very low	8.962	32639	61.88	1	Syiah Kuala
3	Medium	0.735	2676	5.075		
4	High	0.022	80	0.15		
			52747	**100**		

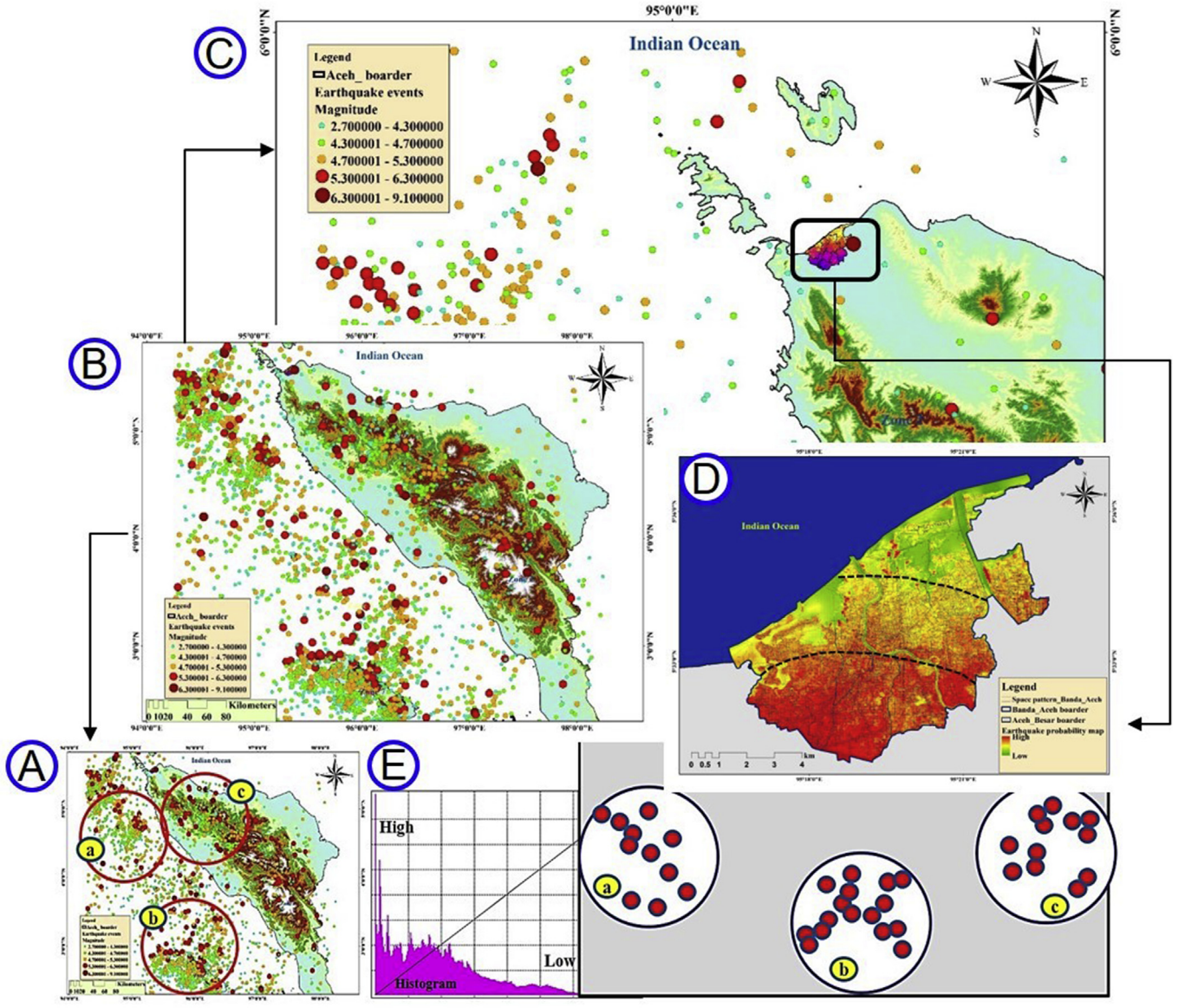

Fig. 13. Validation of earthquake mapping result: (A) Earthquake events in Aceh province (set of earthquakes in different zones of a, b, c); (B) zoomed image of Aceh with earthquakes; (C) position of Banda Aceh and events in Aceh province; (D) earthquake probability map and presented as low to high with the set of earthquakes to validate the Probability result; (E) histogram of probability map that shows the high and low probabilities.

and practical estimation of earthquake risk and provides urban planning information. The drawback of this study is that much time is needed for the model's implementation in a wider-scale region because the ANN process is time-consuming, and it requires a large amount of training data points within the integrated model for probability mapping. The limitations of the proposed scheme include a lack of high-quality infrastructure data and long processing time. Future studies may include the application of artificial intelligence technique and hybrid

models for earthquake risk mapping.

Acknowledgment

This research is funded by Centre for Advanced Modelling and Geospatial Information Systems, University of Technology Sydney: 323930, 321740.2232335 and 321740.2232357.

References

Abraham, A., 2005. Handbook of Measuring System Design. John Wiley and Sons Ltd, Chichester, UK. https://doi.org/10.1002/0471497398.

Adger, W.N., Brooks, N., Bentham, G., Agnew, M., Eriksen, S., 2004. New Indicators of Vulnerability and Adaptive Capacity; Tyndall Centre for Climate Change Research. Final Project Report. University of East Anglia, Norwich, UK, p. 122pp.

Aghataher, R., Delavar, M.R., Nami, M.H., Samnay, N., 2008. A fuzzy-AHP decision support system for evaluation of cities vulnerability against earthquakes. World Appl. Sci. J. 3, 66–72.

Aghdam, I.N., Varzandeh, M.H.M., Pradhan, B., 2016. Landslide susceptibility mapping using an ensemble statistical index (Wi) and adaptive neuro-fuzzy inference system (ANFIS) model at Alborz Mountains (Iran). Environ. Earth Sci. 75 (7), 553. https://doi.org/10.1007/s12665-015-5233-6.

Alarifi, A.S., Alarifi, N.S., Al-Humidan, S., 2012. Earthquakes magnitude predication using artificial neural network in northern Red Sea area. J. King Saud Univ. Sci. 24, 301–313.

Alizadeh, M., Ngah, I., Hashim, M., Pradhan, B., Pour, A., 2018a. A hybrid analytic network process and artificial neural network (ANP-ANN) model for urban earthquake vulnerability assessment. Remote Sens. 10, 975.

Alizadeh, M., Hashim, M., Alizadeh, E., Shahabi, H., Karami, M., Beiranvand Pour, A., Pradhan, B., Zabihi, H., 2018b. Multi-criteria decision making (MCDM) model for seismic vulnerability assessment (SVA) of urban residential buildings. ISPRS Int. J. Geo-Inf. 7, 444.

Armaş, I., 2012. Multi-criteria vulnerability analysis to earthquake hazard of Bucharest, Romania. Nat. Hazards 63, 1129–1156.

Atkinson, P.M., Tatnall, A.R.L., 1997. Introduction neural networks in remote sensing. Int. J. Remote Sens. 18, 699–709.

Bahadori, H., Hasheminezhad, A., Karimi, A., 2017. Development of an integrated model for seismic vulnerability assessment of residential buildings: application to Mahabad City. Iran. J. Build Eng. 12, 118–131.

Bathrellos, G.D., Skilodimou, H.D., Chousianitis, K., Youssef, A.M., Pradhan, B., 2017. Suitability estimation for urban development using multi-hazard assessment map. Sci. Total Environ. 575, 119–134.

Beccari, B.A., 2016. Comparative analysis of disaster risk, vulnerability and resilience composite indicators. PLOS Currents 8. https://doi.org/10.1371/currents.dis.453df025e34b682e9737f95070f9b970.

Bellier, O., Sébrier, S., Pramumijoyo, T., Beaudouin, H., Harjono, I., Bahar, O., 1997. Fomi. Paleoseimicity and seismic hazard along the ornat Sumatran Fault (Indonesia). J. Geodyn. 24, 169–183.

Bilham, R., Ambrasey, N., 2005. Apparent Himalayan slip deficit from the summation of seismic moments for Himalayan earthquakes, 1500–2000. Curr. Sci. 88, 1658–1663.

Birkmann, J., 2007. Risk and vulnerability indicators at different scales: applicability, usefulness and policy implications. Environ. Hazards 7, 20–31.

Birkmann, J., Welle, T., 2015. Assessing the risk of loss and damage: exposure, vulnerability and risk to climate-related hazards for different country classifications. Int. J. Glob. Warming 8, 191–212.

Brebbia, C., Beskos, D., Kausel, E., 1996. The Kobe Earthquake: Geodynamical Aspects. Computational Mechanics Publications, Southampton, p. 160.

Chaulagain, H., Rodrigues, H., Silva, V., Spacone, E., Varum, H., 2015. Seismic risk assessment and hazard mapping in Nepal. Nat. Hazards 78, 583–602.

Culshaw, M.G., Duncan, S.V., Sutarto, N.R., 1979. Engineering geological mapping of the Banda Aceh alluvial basin, northern Sumatra, Indonesia. Bulletin of the International Association of Engineering Geology-Bulletin de l'Association Internationale de Géologie Bull. Int. Assoc. Eng. Geol. Bull. Assoc. Int. Géol. 19, 40–47.

Cutter, S.L., 1996. Vulnerability to environmental hazards. Prog. Hum. Geogr. 20, 529–539.

Davidson, R., Shah, H.C., 1997. A multidisciplinary urban earthquake disaster risk index. Earthq. Spectra 13, 211–223.

Davidson, D., Freudenburg, W., 1996. Gender and environmental risk concerns. Environ. Behav. 28, 302–339.

Davidson, R.A., 1997. An urban earthquake disaster risk index. The John A. Blume Earthquake Engineering Center Report No. 121. Blume Center, Stanford, CA, USA, p. 269.

D'Ayala, D.F., Carriero, A., Sabbadini, F., Fanciullacci, D., Ozelik, P., Akdogan, M., Kaya, Y., 2008. Seismic Vulnerability and Risk Assessment of Cultural Heritage Buildings in Istanbul, Turkey. 14th, vol. 3. WCEE, Beijing.

Dimri, S., Lakhera, R.C., Sati, S., 2007. Fuzzy-based method for landslide hazard assessment in active seismic zone of Himalaya. Landslides 4, 101.

Fanos, A.M., Pradhan, B., 2019. A Spatial Ensemble Model for Rockfall Source Identification From High Resolution LiDAR Data and GIS. IEEE Access 7, 74570–74585. https://doi.org/10.1109/ACCESS.2019.2919977.

Gitamandalaksana, 2009. Final report: identification of seismic source's zone and tsunami hazard probability as considerations in development policy of Banda Aceh city. Nanggroe Aceh Darussalam Province (Package-1), Banda Aceh 33pp.

Gong, P., 1996. Integrated analysis of spatial data for multiple sources: using evidential reasoning and artificial neural network techniques for geological mapping. Photogramm. Eng. Remote Sens. 62, 513–523.

Granger, K., Jones, T., Leiba, M., Scott, G., 1999. Community Risk in Cairns: A Provisional Multi- Hazard Risk Assessment; AGSO Cities Project Report No. 1. Australian Geological Survey Organisation, Canberra, Australia, p. 231.

Gulkan, P., Sozen, M.A., 1999. Procedure for determining seismic vulnerability of building structures. Struct. J. 96, 336–342.

Hagan, M.T., Demuth, H.B., Beale, M., 1996. Neural Network Design. PWS Publication, Boston, MA, USA, p. 1012.

Hosseini, A., GHasemi, Z., Ahadnejad, M., Alimoradi, T., 2014. Evaluation of qualitative and quantitative indicators of social housing in the Tabriz metropolitan. Int. J. Bus. Behav. Sci. 4, 19–30.

Indonesia State Ministry for National Planning Development Agency/BAPPENAS, 2005. Preliminary Damage and Loss Assessment-The December 26, Natural Disaster. Government Printer, Jakarta, p. 128.

Irwansyah, E., 2010. Building damage assessment using remote sensing, aerial photograph and GIS data: case study in Banda Aceh after Sumatera earthquake 204. In: Proceeding of the 11th Seminar on Intelligent Technology and Its Application-SITIA, 11, p. 57.

Johar, F., Majid, M.R., Jaffar, A.R., Yahya, A.S., 2013. Seismic microzonation for Banda Aceh city planning. Plan. Malays. J 11, 1–26.

Kafle, S.K., 2006. Rapid disaster risk assessment of coastal communities: a case study of mutiara village, Banda Aceh, Indonesia. In: Proceedings of the International Conference on Environment and Disaster Management Held in Jakarta, Indonesia on December, pp. 5–8.

Karimzadeh, S., Kadas, K., Askan, A., Erberik, M.A., Yakut, A., 2017. A study on fragility analyses of masonry buildings in Erzincan (Turkey) utilizing simulated and real ground motion records. Procedia. Eng. 199, 188–193.

Karunanithi, N., Grenney, W.J., Whitley, D., Bovee, K., 1994. Neural networks for river flow prediction. J. Comput. Civ. Eng. 8 (2), 201–220.

Khan, S., 2012. Vulnerability assessments and their planning implications: a case study of the Hutt Valley, New Zealand. Nat. Hazards 64, 1587–1607.

Khan, S.A., Pilakoutas, K., Hajirasouliha, I., Garcia, R., Guadagnini, M., 2018. Seismic risk assessment for developing countries: Pakistan as a case study. Earthq. Eng. Eng. Vib. 17, 787–804.

Lin, P.S., Lee, C.T., 2008. Ground-motion attenuation relationships for subduction zone earthquakes in northeastern Taiwan. Bull. Seismol. Soc. Am. 98, 220–240.

Martins, V.N., Silva, D.S., Cabral, P., 2012. Social vulnerability assessment to seismic risk using multicriteria analysis: the case study of Vila Franca do Campo (São Miguel Island, Azores, Portugal). Nat. Hazards 62, 385–404.

McIlraith, A.L., Card, H.C., 1997. Birdsong recognition using backpropagation and multivariate statistics. IEEE Trans. Signal Process. 45, 2740–2748.

Mili, R.R., Hosseini, K.A., Izadkhah, Y.O., 2018. Developing a holistic model for earthquake risk assessment and disaster management interventions in urban fabrics. Int. J. Disaster Risk. Reduct. 27, 355–365.

Mohammady, M., Pourghasemi, H.R., Pradhan, B., 2012. Landslide susceptibility mapping at Golestan Province, Iran: A comparison between frequency ratio, Dempster–Shafer, and weights-of-evidence models. J. Asian Earth Sci. 61 (15), 221–236. https://doi.org/10.1016/j.jseaes.2012.10.005.

Morales-Esteban, A., Martínez-Álvarez, F., Reyes, J., 2013. Earthquake prediction in seismogenic areas of the Iberian Peninsula based on computational intelligence. Tectonophysics 593. https://doi.org/10.1016/j.tecto.2013.02.036.

Nedic, V., Despotovic, D., Cvetanovic, S., Despotovic, M., Babic, S., 2014. Comparison of classical statistical methods and artificial neural network in traffic noise prediction. Environ. Impact Assess. Rev. 49, 24–30.

Oliveira, C.S., 2003. Seismic vulnerability of historical constructions: a contribution. Bull. Earthq. Eng. 1, 37–82.

Panahi, M., Rezaie, F., Meshkani, A.S., 2014. Seismic vulnerability assessment of school buildings in Tehran city based on AHP and GIS. Nat. Hazards Earth Syst. Sci. 14, 969–979.

Panakkat, A., Adeli, H., 2007. Neural network models for earthquake magnitude prediction using multiple seismicity indicators. Int. J. Neural Syst. 17, 13–33.

Panakkat, A., Adeli, H., 2009. Recurrent neural network for approximate earthquake time and location prediction using multiple seismicity indicators. Comput. Aided Civ. Infrastruct. Eng. 4, 280–292.

Paola, J.D., Schowengerdt, R.A., 1995. A review and analysis of backpropagation neural networks for classification of remotely-sensed multi-spectral imagery. Int. J. Remote Sens. 16, 3033–3058.

Pay, C., 2001. A new methodology for the seismic vulnerability assessment of existing buildings in Turkey. M.Sc. thesis. Middle East Technical University, Ankara.

Pradhan, B., Hasan, H.A., Jebur, M.N., Tehrany, M.S., 2014. Land subsidence susceptibility mapping at Kinta Valley (Malaysia) using the evidential belief function model in GIS. Nat. Hazards 73 (2), 1019–1042. https://doi.org/10.1007/s11069-014- 1128-1.

Pradhan, B., Jena, R., 2016. Spatial relationship between earthquakes, hot-springs and faults in Odisha, India. In: IOP Conference Series: Earth and Environmental Science, vol. 37. IOP Publishing, 012070.

Pradhan, B., Lee, S., 2009. Landslide risk analysis using artificial neural network model focussing on different training sites. Int. J. Phys. Sci. 4, 1–15.

Pradhan, B., Lee, S., 2010. Regional landslide susceptibility analysis using back-propagation neural network model at Cameron Highland, Malaysia. Landslides 7 (1), 13–30. https://doi.org/10.1007/s10346-009-0183-2.

Pradhan, B., Moneir, A.A.A., Jena, R., 2018. Sand dune risk assessment in Sabha region, Libya using Landsat 8, MODIS, and Google Earth Engine images. Geomatics, Nat. Hazards Risk 9, 1280–1305.

Ram, T.D., Wang, G., 2013. Probabilistic seismic hazard analysis in Nepal. Earthq. Eng. Eng. Vib. 12, 577–586.
Rashed, T., Weeks, J., 2003. Assessing vulnerability to earthquake hazards through spatial multicriteria analysis of urban areas. Int. J. Geogr. Inf. Sci. 17, 547–576.
Rygel, L., O'Sullivan, D., Yarnal, B.A., 2006. Method for constructing a social vulnerability index: an application to hurricane storm surges in a developed country. Mitig. Adapt. Strategies Glob. Change 11, 741–764.
Saaty, T.L., 2013. Analytic hierarchy process. In: Encyclopedia of Operations Research and Management Science. Springer, Boston, MA, pp. 52–64.
Setiawan, B., 2017. Site specific ground response analysis for quantifying site amplification at a regolith site. Ind. J. Geoscience 4, 159–167.
Setiawan, B., Jaksa, M., Griffith, M., Love, D., 2018. Seismic site classification based on constrained modelling of measured HVSR curve in regolith sites. Soil Dyn. Earthq. Eng. 110, 244–261.
Shimizu, S., Sugisaki, K., Ohmori, H., 2008. Recursive sample-entropy method and its application for complexity observation of earth current. In: International Conference on Control, Automation and Systems (ICCAS). Seoul, South Korea, pp. 1250–1253.
Siemon, B., Ploethner, D., Pielawa, J., 2005. Hydrogeological Reconnaissance Survei in the Province Nanggroe Aceh Darussalam Northern Sumatra, Indonesia Survei Area: Banda Aceh/Aceh Besar 2005, Report C 1, BGR. Federal Institute for Geosciences and Natural Resources.
Soe, M., Ryutaro, T., Ishiyama, D., Takashima, I., Charusiri, K.W.I.P., 2009. Remote sensing and GIS based approach for earthquake probability map: a case study of the northern Sagaing fault area, Myanmar. J. Geol. Soc. Thail. 29–46.
Sørensen, M., Atakan, K., 2008. Continued earthquake hazard in Northern Sumatra: Potential effects of a future earthquake. EOS. Trans. Am. Geophys. Union 89, 133–134.
Tehrany, M.S., Pradhan, B., Jebur, M.N., 2014. Flood susceptibility mapping using a novel ensemble weights-of-evidence and support vector machine models in GIS. J. Hydrol. 512, 332–343. https://doi.org/10.1016/j.jhydrol.2014.03.008.
Tien Bui, D., Ho, T.C., Pradhan, B., Pham, B.-T., Nhu, V.-H., Revhaug, I., 2016. GIS-based modeling of rainfall-induced landslides using data mining-based functional trees classifier with AdaBoost, Bagging, and MultiBoost ensemble frameworks. Environ. Earth Sci. 75, 1101. https://doi.org/10.1007/s12665-016-5919-4.
Tierney, K., 2006. Social inequality: humans and disasters. In: Daniels, R.J., Keitl, D.F., Kunreuther, H. (Eds.), On Risk and Disaster: Lessons from Hurricane Katrina. University of Pennsylvania Press, Philadelphia, PA, USA. https://doi.org/10.9783/9780812205473.109.
Turmov, G.P., Korochentsev, V.I., Gorodetskaya, E.V., Mironenko, A.M., Kislitsin, D.V., Starodubtsev, O.A., 2000. Forecast of underwater earthquakes with a great degree of probability. In: Proceedings of the 2000 International Symposium on Underwater Technology. Tokyo, Japan, pp. 110–115.
Turner, B.L., Kasperson, R.E., Matson, P.A., McCarthy, J.J., Corell, R.W., Christensen, L., Eckley, N., Kasperson, J.X., Luers, A., Martello, M.L., Polsky, C., Pulsipher, A., Schiller, A., 2003. A framework for vulnerability analysis in sustainability science. Proc. Natl. Acad. Sci. U.S.A. 100, 8074–8079.
Wang, K., Chen, Q.F., Sun, S., Wang, A., 2006. Predicting the 1975 Haicheng earthquake. Bull. Seismol. Soc. Am. 96, 757–795.
Wisner, B., Blaikie, P., Cannon, T., Davis, I., 2003. At Risk: Natural Hazards, People's Vulnerability and Disasters, second ed. Routledge, Abingdon, UK, pp. 11–13.
Xu, C., Dai, F.C., Xu, X.W., 2010. Wenchuan earthquake-induced landslides: an overview. Geol. Rev. 56, 860–874 (in Chinese with English abstract).
Yakut, A., Aydogan, V., Ozcebe, G., Yucemen, M.S., 2003. Preliminary seismic vulnerability assessment of existing reinforced concrete buildings in Turkey. Seismic Assessment and Rehabilitation of Existing Buildings. Springer, Dordrecht, pp. 43–58.
Youngs, R.R., Silva, W.J., Humprey, J.R., 1997. Seismol. Res. Lett. 68, 1.
Youssef, A.M., Al-Kathery, M., Pradhan, B., 2015. Landslide susceptibility mapping at Al-Hasher area, Jizan (Saudi Arabia) using GIS-based frequency ratio and index of entropy models. Geosci. J. 19 (1), 113–134. https://doi.org/10.1007/s12303-014-0032-8.
Yücemen, M.S., Özcebe, G., Pay, A.C., 2004. Prediction of potential damage due to severe earthquakes. Struct. Saf. 26, 349–366.
Yuzal, H., Kim, K., Pant, P., Yamashita, E., 2017. Tsunami evacuation buildings evacuation planning in Banda Aceh, Indonesia. J. Emerg. Manag. 15, 49–61.
Zare, M., Pourghasemi, H.R., Vafakhah, M., Pradhan, B., 2013. Landslide susceptibility mapping at VazWatershed (Iran) using an artificial neural networkmodel: a comparison between multilayer perceptron (MLP) and radial basic function (RBF) algorithms. Arab. J. Geosci. 6 (8), 2873–2888. https://doi.org/10.1007/s12517-012-0610-x.
Zebardast, E., 2013. Constructing a social vulnerability index to earthquake hazards using a hybrid factor analysis and analytic network process (F'ANP) model. Nat. Hazards 65, 1331–1359.
Zhang, J.S., Jia, Z.K., 2010. The study on assessment index of urban social vulnerability to the earthquake disaster. Technological Guide 36, 12–14.
Zhang, Y., van den Berg, A.E., Dijk, T.V., Weitkamp, G., 2017. Quality over quantity: contribution of urban green space to neighborhood satisfaction. Int. J. Environ. Res. Public Health 14, 535.
Zhao, Y., Takano, K., 1999. An artificial neural network approach for broadband seismic phase picking. Bull. Seismol. Soc. Am. 89, 670–680.
Zhihuan, Z., Junjing, Y., 1990. Prediction of earthquake damages and reliability analysis using fuzzy sets. In: First International Symposium on Uncertainty Modeling and Analysis. College Park, MD, USA, pp. 173–176.